SPECIFIC ION EFFECTS ON INTERFACIAL PHENOMENA

A Dissertation

by

SARAH CECILIA FLORES ARAUJO

Submitted to the Office of Graduate Studies of
Texas A&M University
in partial fulfillment of the requirements for the degree of

DOCTOR OF PHILOSOPHY

December 2011

Major Subject: Chemistry

Specific Ion Effects on Interfacial Phenomena

Copyright 2011 Sarah Cecilia Flores Araujo

SPECIFIC ION EFFECTS ON INTERFACIAL PHENOMENA

A Dissertation

by

SARAH CECILIA FLORES ARAUJO

Submitted to the Office of Graduate Studies of
Texas A&M University
in partial fulfillment of the requirements for the degree of

DOCTOR OF PHILOSOPHY

Approved by:

Chair of Committee,	Paul S. Cremer
Committee Members,	David P. Barondeau
	David H. Russell
	Alexei Sokolov
Head of Department,	David H. Russell

December 2011

Major Subject: Chemistry

ABSTRACT

Specific Ion Effects on Interfacial Phenomena.

(December 2011)

Sarah Cecilia Flores Araujo, B.S.; M.S., University of North Texas

Chair of Advisory Committee: Dr. Paul S. Cremer

A new interdisciplinary facet of chemistry has developed, as we attempt to comprehend complex interfacial phenomena in which ions play crucial roles. Understanding the mechanisms by which ions affect water at surfaces and interact with the molecules dissolved in it, pose a ubiquitous challenge with enormous implications for biological and physical sciences. These represent steps towards unraveling mechanisms in protein folding and crystallization, protein-protein interactions, enzymatic activity, implant biocompatibility, atmospheric chemistry phenomena, and even in more inorganic processes like metal oxide dissolution and corrosion; all of them fundamental technological challenges.

In this thesis, the specific ion effects on interfacial water structure adjacent to air/water and solid/water interfaces were explored using vibrational sum frequency spectroscopy. At the air/water interface, monolayers of bovine serum albumin, elastin-like peptides, and surfactants, were analyzed in presence of subphases that consisted of different sodium salts and varying pH value. The results suggested that anions interact directly with the protein's surface, and their effects on water structure are dominated by

the charge state of the interfacial layer, rather than the detailed chemical structure of the macromolecules. At the solid/liquid interface, water structure at surfaces like quartz, octadecyltrichlorosilane-covered quartz, and titanium oxide, confirmed that the propensities of anions to adsorb at an interface are favored for more polarizable anions, following the Hofmeister order, and disproving the notion that the order of the interaction can be inverted with changes in charge sign or degree of hydrophobicity of the surface.

Similarly, by analyzing interfacial water structure we performed one of the very first systematic studies on the interactions of cations with metal oxide surfaces. The results showed that specific cation effects were quite prominent at low concentration and high pH value, following a direct Hofmeister series, which can be explained in terms of charge density, polarizability, and basicity of the oxide surfaces.

Our findings are of interest, since they provide with essential information not only to understand protein phenomena associated with neurodegenerative conditions like Alzheimer, but also by proving the generality of ion interactions beyond biological, we can even influence the development of the next generations of microprocessors and beyond.

DEDICATION

To My Family

ACKNOWLEDGEMENTS

I would like to thank my committee chair, Prof. Paul S. Cremer for his trust, guidance and support throughout the course of this research, as well as to my committee members, Prof. Barondeau, Prof. Goodman, Prof. Russell, and Prof. Sokolov.

Thanks also go to my colleagues and friends, and the department faculty and staff for making my time at Texas A&M University a unique experience. I also want to extend my gratitude to the National Science Foundation (CHE-0094332), the Welch Foundation (Grant A-1421), and the Consejo Nacional de Ciencia y Tecnología (México, scholarship No. 210738), which provided funding and financial support during my doctorate studies. To Prof. Chen, and Dr. Cimatu for sharing their knowledge, as well as Dr. Kherb for his unconditional help. Additionally, thanks to Prof. Ashutosh Chilkoti for supplying the DNA plasmids from which the elastin-like peptides were made.

I also would like to acknowledge Dr. Mendoza (R. I. P.) who instructed me at the onset of this journey, and Prof. Chyan for his continuing support throughout the completion of my bachelor and master studies.

Finally, thanks to my family for their encouragement and patience, and to my husband for his endless support and love.

TABLE OF CONTENTS

CHAPTER Page

LIST OF FIGURES

FIGURE Page

CHAPTER I

INTRODUCTION

Specific Ion Effects and the Hofmeister Series

The Hofmeister series involves the specific effects of ions in solution, and originally described the order in which they were able to influence the solubility of proteins and colloidal systems.[1] Since its discovery in 1888 by Franz Hofmeister, it has been found that there are consistent effects influencing a wide range of physical phenomena, which includes both biological and inorganic systems.[2] For example, specific ion effects have been observed in protein stability,[3,4] enzyme activity,[5-8] protein-protein interactions,[9,10] protein crystallization,[11] optical rotation of sugars and amino acids,[12] bacterial growth,[13] surface tension of aqueous interfaces,[14,15] micelle formation,[16-18] membrane permeability,[19] the phase behavior of monolayers and macromolecules,[20-23] water retention by wool fibers,[24] and less biological phenomena like precipitation of inorganic nanoparticles and zeolites, for which its size, morphology and structure depend on specific ion effects.[25]

Originally, Hofmeister ranked anions and cations according to their ability to salt-in or salt-out proteins in aqueous solutions.[26] It was found that anions in particular have a very pronounced influence on the solubility of proteins, and their effects are now correlated to their ability to interact with protein surfaces in solution. [22,27]

This dissertation follows the style of *Journal of the American Chemical Society*.

The direct order in which the Hofmeister anions influence the solubility of proteins is the following:

$$SCN^- > ClO_4^- > Br^- > NO_3^- > Cl^- > SO_4^{2-}$$

The ions on the left are known as chaotropes, and the ions on the right are known as kosmotropes. The chaotropic anions are known to decrease protein stability and increase their solubility; in addition they decrease the surface tension and increase the protein denaturation. In contrast, the kosmotropic anions have the opposite effects and salt-out proteins from solution. Generally, the larger, more polarizable anions tend to be chaotropic, and the smaller ions, which are generally better solvated, behave as kosmotropes.

For cations, the usual order in which these affect the stability of proteins is as follows:

$$Cs^+ > Rb^+ > NH_4^+ > K^+ > Na^+ > Li^+ > Ca^{2+} > Mg^{2+} > Zn^{2+}$$

The ions on the left tend to stabilize the native folded structure of a protein and decrease solubility, while the ions on the right tend to facilitate protein denaturation and increase solubility.[28] For cations, the definitions of chaotropes (left) and kosmotropes (right) are valid on completely hydrophobic molecules, and they tend to have opposite effects for polar systems in the sense that kosmotropes are the ones that interact more with the proteins and increase the protein denaturation. Commonly, at relatively hydrophobic interfaces such as protein surfaces, the effects of anions tend to be more pronounced than those of cations, and therefore are easier to monitor.[29-31] As a result there are fewer experimental studies exploring the interactions of cations with similar systems.[24,32-33] For

both ion series, the approximate neutral case or "null point" between chaotropes and kosmotropes is considered to be Cl^- for the anions and Na^+ for the cations, which varies as well, depending on the properties of the systems they are interacting with.

A molecular level understanding of the specific ion effects is just developing. In early days it was believed that the effect observed by Hofmeister originated from the change in hydrogen-bonding network in bulk water with the addition of salt.[28,34] Chaotropes were considered as water structure breakers that would weaken the aqueous hydrogen bonding, while kosmotropes were thought to be water structure makers. Therefore, it made sense that by affecting the water structure around them, ions would influence the chemistry of the solution (Figure 1.1A).

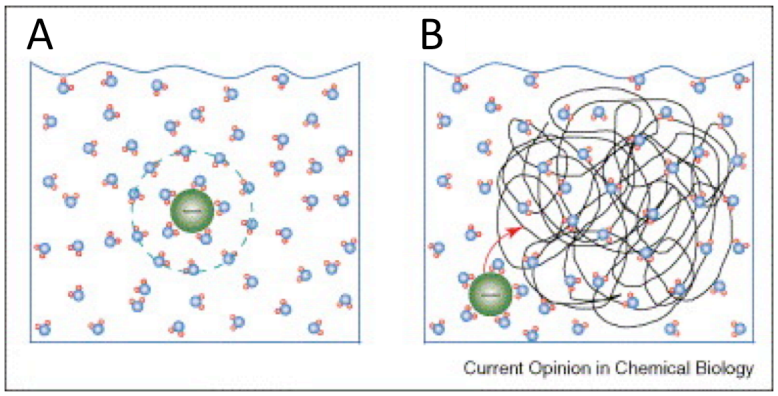

Figure 1.1 Anions and water structure.[35] A) Organized water beyond an anion's first hydration shell would be needed for structure-making and breaking effects to occur. B) The direct interaction of an anion with a macromolecule in aqueous solution. The relative sizes of ions and molecules are not generally to scale. However, the relative size of the anion with respect to the water molecules is approximately correct for SO_4^{2-}.

However recent experimental and theoretical investigations have demonstrated that bulk water structure making and breaking abilities of salts is not central to the Hofmeister effect.[36] It has been demonstrated that ions do not affect water structure beyond their first hydration shell, and therefore are unable to influence water hydrogen bond network in a way to induce ion-biomolecule interactions.[37] These observations have led to a hypothesis that considers the Hofmeister effect as an interfacial behavior, which involves the direct interactions of ions with the macromolecule's aqueous interface (Figure 1.1B).[30]

A wide variety of spectroscopic, thermodynamic, and computational studies have been conducted to study the effects of anions at uncharged and charged interfaces.[22,23,27,38-40] Several review articles summarize these findings, and generally a Hofmeister sequence is observed for a wide variety of processes.[1,2,41] Theoretical calculations have been extremely relevant in predicting and corroborating the direct interaction of larger and more polarizable anions with protein surfaces.[42-44] It has been basically demonstrated that less hydrated anions have a preference for the interfacial region. Other calculations employed a salt ion-partitioning model (SPM) to interpret and predict Hofmeister ion effects at the air/water and protein/water interfaces. These studies also showed that more chaotropic anions usually partition to the interface to a greater extent than other species.[45-47] Experimentally, our laboratory studied the effects of anions on octadecylamine (ODA) Langmuir monolayers.[48] These studies demonstrated that the physical properties of the monolayer follow a direct Hofmeister series as noted by the effect on the ordering of the monolayer. Furthermore, measurement of the lowest

critical solution temperature (LCST) for a neutral polymer poly(*N*-isopropylacrylamide) (PNIPAM) indicates that chaotropic anions in fact decrease the polymer's stability and increase its solubility, and the overall effect in the LCST follows the Hofmeister order.[22] These experiments support the notion that anions bind directly to macromolecules. All the evidence above suggests that bulk water structure making and breaking are not responsible for phenomena related to the Hofmeister series, although further experiments with real protein systems are still necessary.

Particularly, in our laboratory, the observation of the effects of ions at interfaces has been facilitated by the use of surface specific vibrational sum frequency spectroscopy (VSFS), which will be described in detail in Chapter II. VSFS was used to observe the effects of anions by analyzing vibrational water spectra obtained at the air/water interface. Since the VSFS signal is proportional to the square of the surface potential, we can observe the changes in overall surface charge promoted by the adsorption of anions, by monitoring changes in the intensity of the water spectra. The VSFS signal derives from a few water layers adjacent to the macromolecule aqueous interface, or the surface in question, and its intensity is proportional to the amount of water molecules oriented by the available electric fields. For example, the Hofmeister effects observed on PNIPAM have been confirmed with VSFS, in a study that demonstrates the preferential partition of more chaotropic anions to the PNIPAM/water interface, as demonstrated by the more intense water spectra.[27] In Chapter III, the VSFS water spectra in presence of bovine serum albumin (BSA), elastin-like peptides (ELPs), and surfactants or amphiphilic molecules, is presented as further evidence for the direct

interaction of anions with these macromolecules. This study involves a real model protein, and the results are significant in demonstrating that for sufficiently charged proteins and macromolecules, the nature of the interaction is electrostatic and depends on the charge of the monolayer rather than its detailed chemical structure.[27,30] In this recent study, the effects of anions on water structure demonstrate an inversion in the Hofmeister effects as the protein in solution is below its isoelectric point. Therefore, these experiments demonstrate an inversion of the anionic Hofmeister series, particularly when the proteins under study are below their isoelectric point, or are positively charged.[29,49,50] Another example is the case of lysozyme protein, which aggregation at low salt concentrations (< 200~300 mM) follows an inverse Hofmeister series. As the salt concentration is increased (> 300 mM) the order is reverted to a direct series.[29] Although in these studies, the effects on water structure and LCST are inversed, it is important to point out that the adsorption of anions is still direct, and chaotropes like SCN^- and ClO_4^- are interacting preferentially with the protein surface. In Chapter IV we investigated the effect of the Hofmeister anions on quartz and TiO_2, which are used as model negative and positively charged hydrophilic surfaces, in order to understand the interaction of anions with interfaces where surface charge is one of the main factors dominating the phenomenon. On the other hand, we also investigated the effects of anions on octadecyltrichlorosilane (OTS) covered quartz, and lysozyme Gibbs monolayers, which are representative of hydrophilic surfaces with certain hydrophobic character, bearing negative and positive charge respectively. From the results of our experiments, it is evident that the order of interactions of anions with surfaces of

opposite charge and varying degree of hydrophilicity follows a direct Hofmeister series. Even if the overall Hofmeister effect appears direct or inverse, we demonstrated that adsorption of anions to aqueous interfaces is still favored for chaotropic anions, regardless of changes in sign or degree of hydrophilicity of the surfaces.

Similarly, by analyzing changes in the intensity of the VSFS water spectrum at the solid/liquid interface, in Chapter V we obtain information about the extent of interactions between cations and hydrophilic negatively charged surfaces in solution. The main purpose of this Chapter is to understand the effects of cations by monitoring their adsorption to relatively simple interfaces that are purely negatively charged. We provide a systematic study on the interaction of various alkali, alkali earth, and transition metal cations with quartz and titanium dioxide. Our observations provide clear evidence of the significance of the interactions between cations and purely negatively charged surfaces. The interactions vary with the intrinsic properties of the substrates as well as the individual nature of the cations, occurring in the same order as predicted by Hofmeister. We demonstrate a clear correlation between surface polarizability and the preferred order of interactions of cations at hydrophilic interfaces. The use of these relatively simple systems in which we isolate charge interactions from other factors such as hydrophobic interactions and structural complexity, may aide in understanding the mechanisms by which Hofmeister cations interact with more complex systems such as peptides and proteins, which up to this day remain unsolved.

Understanding ion interactions with surfaces, and their specific effects on various physical phenomena is central to solve very important challenges in biological and

inorganic fields. For example, it has been observed that as the presence of different salts affect protein stability and enzyme activity, protein misfolding is in turn influenced, which is the origin of diseases and neurodegenerative conditions like Alzheimer. Better understanding of how ion type and concentration affect these phenomena can lead towards the cure of these diseases. Other technological implications, are for example in the semiconductor industry, in which molecular level understanding of ion interactions can lead to enhancement of chemical mechanical polishing methods in the fabrication of integrated circuits, or development of new materials that can satisfy the miniaturization demands. This is imperative as the processes continue and approach the limits in semiconductor manufacturing. Furthermore, other areas like biomedical can be greatly influenced by our investigations as we provide with molecular level information that facilitates the understanding of why certain materials are good as implants, and demonstrate enhanced biocompatibility.

CHAPTER II

VIBRATIONAL SUM FREQUENCY SPECTROSCOPY

Principles

Vibrational sum-frequency spectroscopy (VSFS) has been used in our laboratory due to its inherent surface specificity.[27,30] VSFS is based on the non-linear optical phenomenon sum frequency generation (SFG) in which two photons combine to generate a third photon, whose frequency is the summation of the frequencies of the photons from the two incident beams (Figure 2.1).[51]

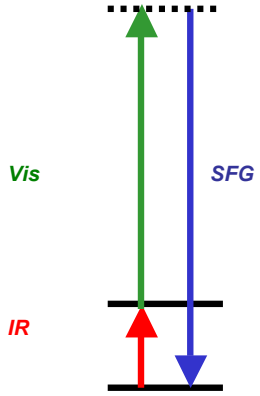

Figure 2.1 Energy diagram of vibrational sum frequency spectroscopy (VSFS).

Usually one of the photons comes from an infrared source and the other from a visible beam. The probability of obtaining a sum frequency response is significantly

enhanced when the frequency of the infrared beam is in resonance with the molecular vibrations of the sample. The sum frequency response is proportional to the intensity of the visible and infrared beams.

$$I_{SFG} = \left|\chi^{(2)}\right|^2 \times I_{IR} \times I_{Vis} \tag{1}$$

The term $|\chi^{(2)}|$ refers to the effective second order nonlinear susceptibility of the sample, and it is only observed in materials that are noncentrosymmetric, which is a characteristic of surfaces and interfaces. The term $|\chi^{(2)}|$ is composed of a frequency-independent nonresonant term $\chi_{NR}^{(2)}$ and a frequency-dependent resonant term $\chi_R^{(2)}$, which at the same time is proportional to A_q, ω_{IR}, ω_q, and Γ_q, the oscillator strength, the frequency of the input IR beam, the resonant frequency, and the peak width of the qth resonant mode, respectively.

$$\chi_{eff}^{(2)} = \chi_{NR}^{(2)} + \chi_R^{(2)} = \chi_{NR}^{(2)} + \sum_q \frac{A_q}{\omega_{IR} - \omega_q + i\Gamma_q} \tag{2}$$

The sum frequency generation signal provides vibrational information of molecules, which is useful in determining the identity of the functional groups at the interface of interest, and the intensity of the signal can be correlated to the number of oscillators or molecules that are present, as well as to the relative order and net orientation of the vibrating molecules.[52,53]

Experimental Setup

Nd:YAG Laser System

Our VSFS experimental setup consists of a custom made 17 ps pulsed, 1064 nm active/passive mode-locked Nd:YAG laser, with a 50 mJ beam, and rate ~ 20 Hz (Continuum model PY61, Santa Clara, CA). The laser has two main components, an optical bench and the power supply. The optical bench consists mainly of a single flashlamp pumped oscillator, an amplifier pumped by two flashlamps in a close-coupled configuration, and a Q-switch dye pump package DCP-03. The flashlamps in the optical bench are typically replaced every 20,000,000 pulses. The Q-Switch dye purchased from Exciton (Dayton, OH) is dissolved in purified organic solvent 1,2-dichloroethane (99+%, Acros Organics; Geel, Belgium). The dye should be replaced when the level in the container is close to half of the container, or when the operational threshold reaches ~ 1.39 V, which might cause laser power fluctuations and decreased signal to noise ratio. Room temperature must be constant at 24° C to ensure proper optical head performance and flashlamps warm up, as well as to avoid power fluctuations. The power supply energizes the optical head, and provides the logic functions necessary to operate the laser. It also supplies the cooling capacity to get rid of the heat generated in the optical bench by the operation of the flashlamps. A deionized water reservoir cools the flashlamps, which in turn is cooled by an external chilled water system.

The 1064 nm laser beam must have a power of at least 40 mJ in order to pump the combination optical parametric generation and optical parametric amplification system (OPG/OPA), as demonstrated in Figure 2.2.

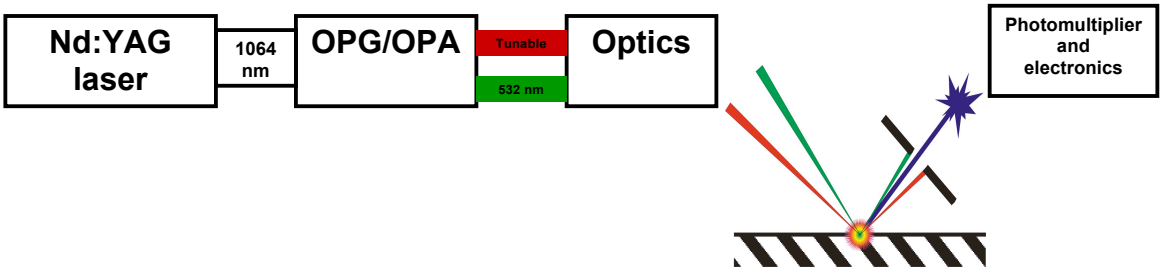

Figure 2.2 Sum frequency vibrational spectroscopy setup.

Optical Parametric Generation and Amplification System

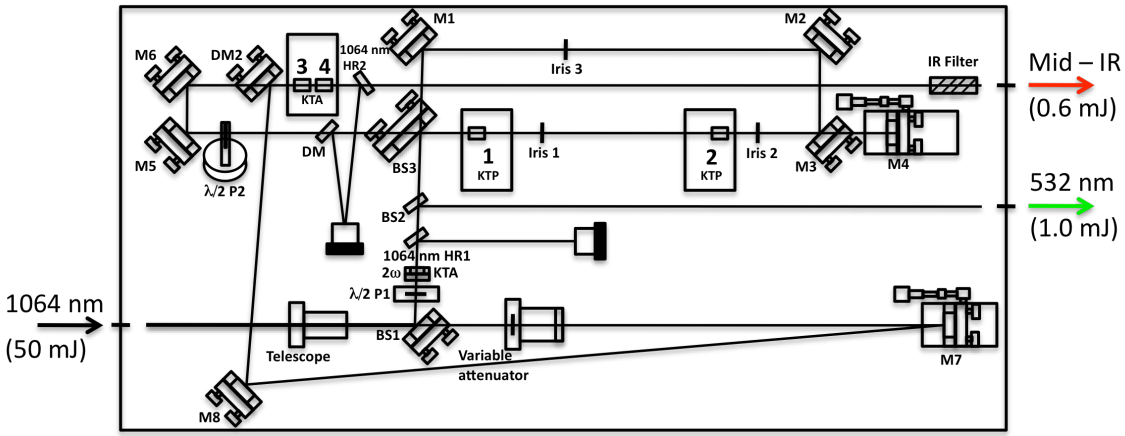

Figure 2.3 Parametric converter system, as configured for mid-infrared generation.

OPG/OPA is a three-wave mixing process, in which a pump beam, a signal beam, and an idler beam at frequencies ω_3, ω_1, and ω_2, propagate and interact in a nonlinear medium.[51] The OPG/OPA system (LaserVision; Bellevue, WA) generates an output infrared and a visible beam through a series of nonlinear KTP and KTA crystals, as will be roughly described in the following paragraphs.

The fundamental 1064 nm laser beam enters the parametric system, and is initially magnified by a telescope as demonstrated in Figure 2.3. The magnified beam is directed towards a beam splitter (BS1) to produce two 1064 nm beams. One of the beams is directed through a variable attenuator, and it is then sent through a delay towards the difference frequency stage (DFG). The second beam goes through a half-wave polarizer, which servers to vary the intensity and maximize the efficiency of the energy conversion process. Then, it is sent through a nonlinear crystal to double the frequency. A high reflectance 1064 nm mirror separates the 1064 nm portion from the generated 532 nm beam and it is sent to a beam dump. The 532 nm beam is further directed through a beam splitter (BS2) and one portion is sent outside the parametric system to be used as the fixed visible beam for the VSFS experiments. The remaining portion of the beam continues towards the OPG/OPA stage, which contains two nonlinear KTP crystals that are mounted in motors 1 and 2. Before entering the first stage, the beam goes through a partial beam splitter (BS3) to obtain two 532 nm beams and pump the crystals from both directions. One of the beams passes through motors 1 and 2, from which two beams of different frequency are generated, the “signal” and the “idler”. The “signal” is a high energy and short wavelength beam, and the “idler” is a

low energy and long wavelength beam. The "idler" continues and the second pass reaching from mirror 4 (M4) is recombined with the portion of 532 nm beam that was sent for a delay through M1, M2, and M3, for the optical parametric amplification process. The "signal" and the residual 532 nm are sent towards a beam dump by a dichroic mirror (DM). The "idler" is directed towards the second stage for the DFG process; the stage has motors 3 and 4 with one KTA crystal each. At this stage, the portion of the 1064 nm beam that was sent for a delay through M7, M8, and DM2, recombines with the "idler" to obtain the new signal and idler. Finally the beam is directed towards a stack-of-plates polarizer, which removes the unwanted signal or idler light, and the overall process leaves a mid-infrared beam tunable from 5 μm to 2.5 μm (2000 cm^{-1} to 4000 cm^{-1}).

The polarization of the three waves involved in the conversion process is determined by the phasematching (momentum conservation) type in use, which is achieved by changing the orientation or angle tuning of the crystal. By rotating the crystals in the extraordinary (e) plane with respect to the incoming beam, the refractive index experienced by light polarized in this plane is changed. This rotational plane contains the optic axis of the crystal; rays parallel to it are termed e-waves, and perpendicular to it are termed o-rays (ordinary). For safety reason, the crystals are configured such that they rotate in the plane parallel to the optical bench, and therefore all e-waves are horizontally polarized and o-waves vertically polarized. The half wave polarizer (λ/2 P2) after the first stage converts the polarization of the "idler" from vertical to horizontal. A type II phase matching condition develops, where the beams are

e-polarized and o-polarized. The birefringent crystals separate the beam in e-rays and o-rays. The "signal" wave is polarized parallel to the rotational plane and is defined e-beam, while the "idler" is defined as the o-beam. As the crystal is rotated, the refractive index for e-polarized waves varies, and the one for o-polarized waves remains unchanged. This difference in positions of the crystals allows the generated infrared beam to be tunable. For both stages, the phase matching condition is type II, in which the phase matching combination for "signal", "idler" and pump beam was eoo (horizontal, vertical, vertical).

Motor Position Optimization and OPG/OPA Alignment

The OPG/OPA system is connected to the computer system, which is equipped with the LaserVision software, which allows manipulation of the motor positions. Prior to each experiment, or if the power is low by 10% to 40% of the expected, the crystals were optimized by scanning each motor through a range of positions to obtain ~ 0.6 mJ of IR power, with a standard deviation near ~ 0.010 mJ. This was done by fixing the frequency at 3200 cm^{-1} with the Master controller, and then tuning each individual motor in the following sequence: motor 2 is adjusted, then motor 3 and then motor 4, followed by motor 3 and finally motor 2 again. Motor 1 should remain in its fixed position to avoid any serious misalignment. At least two optimization cycles were performed as the IR power and standard deviations was measured with an IR sensor (Coherent, Wilsonville, OR). Usually, a series of optimization cycles recovers the IR power before attempting any extensive OPG/OPA alignment.

The alignment of the OPG/OPA system was generally verified when the signal was significantly low (< 50%), or completely absent. Initially, the alignment of the 1064 nm beam was verified along crystals 3 and 4 by observing the beam using an orange neon paper. For proper observation, the path through stage one was blocked with a black cardboard at BS3. The 1064 nm beam must visually appear through the center of crystals 3 and 4. If the beam was not centered, this was achieved by adjusting M7, either horizontally or vertically. To ensure the alignment was correct in a long range, the 1064 nm HR2 and the IR filter were carefully removed, making sure the 1064 nm pump beam was blocked, or the shutter off, to avoid damage of optics. Then the alignment was finely adjusted using M7 to make the 1064 nm beam go through the center of crystals 3 and 4, and DM2 to make the beam go through the center of the pinhole located outside the IR exit (not shown). Generally, alignment is an iterative process in which alternate adjustment is performed for two mirrors until the beam is centered and in plane. Once the 1064 nm is centered through the crystals and the pinhole after the IR outlet, the overlap with the "idler" was verified with the orange neon paper. This was done by reducing the intensity of the 1064 nm beam using the variable attenuator, in order to visually observe the overlap between the 1064 nm and the usually faint "idler", before and after the crystals 3 and 4, and at the pinhole after the IR exit. If the "idler" did not overlap with the 1064 nm, its position was adjusted by alternate tuning of M5 and M6 until visually optimized. The 1064 nm HR2 and the IR filter were placed back in their original positions, and the IR power was measured. This process must recover at least

50% of IR power, although fine adjustment of M5 and M6 while monitoring the signal increase with the IR power meter, was required for 100% IR power.

If the parametric system was misaligned at stage 1, extensive inspection of alignment was done, using irises 1, 2, and 3. Usually, for optimum alignment, the position of the beams at stage 1 is vertically centered in the pinhole, but ~ 1.5 mm off horizontally to the left (from direction of incident beam). Initially, M1 and M8 were covered with a black cardboard piece to avoid further beam propagation. Next, the beam intensity was reduced using λ/2 P1 and the variable attenuator, and the 532 nm beam was aligned through irises 1 and 2 by alternate adjustment of BS1 and BS3 respectively. The brightest center portion of the 532 nm beam must pass through the center of crystals 1 and 2. Once the beam was aligned for crystals 1 and 2, M3 was removed from the path, making sure the beam shutter was off to avoid damage of optics. A black cardboard was used to cover M4 and protect from damage by 532 nm beam from stage 1. Once M3 was removed, the cardboard is removed from M1, and the 532 nm beam is aligned using M1 and M2, through iris 3, and, the reference point in the orange neon paper placed on the side of the OPG/OPA box, in plane with M2 reflection (not shown). Finally, M3 was placed back in the original position, and its alignment was fine tuned so that the reflected 532 nm beam was sent through the irises and the crystals in both directions. The beam profile was verified with the neon paper to ensure the overlap of the beams coming from both directions at each of the irises and crystals. The cardboard was removed from M8, and the intensity of the beams was increased to the original values through λ/2 P1 and the variable attenuator. These steps would recover most of the IR energy; further fine-

tuning must be performed with M5 and M6 to enhance the overlap at the DFG stage. Final steps were to carefully tune M4 to enhance the infrared power, as well as verify the correct position of the IR filter at the outlet of the OPG/OPA.

To perform alignment of motors after changing one of the motors or crystals in the setup, or if there was a major change in the position of the crystals, the steps in the manual were followed to find the new zero positions for all of the motors. Extensive motor position optimization with the LaserVision software was performed until phase matching condition is achieved.

Sample Area and Data Collection

The obtained visible and mid-infrared beams are directed through a series of steering optics before entering the sample area (Figure 2.2). The infrared beam is tunable between 2000 cm^{-1} to 4000 cm^{-1}, and supplies ~ 0.6 mJ per pulse in the CH and OH stretch region. The visible beam is fixed at 532 cm^{-1} providing ~ 1.0 mJ per pulse at the sample surface.

The visible and infrared beams are spatially and temporally aligned through a final set of optics, at either the air/water or solid/water interface depending on the experiment to be performed. In order to investigate the air/water interface, the liquid samples are placed in a small Langmuir trough (Model 601M, NIMA, U. K.) with a volume of 35.0 mL as the one shown in Figure 2.4A. The trough allows measurement and control of the surface pressure, using a Wilhelmy plate and a pair of sliding barriers.

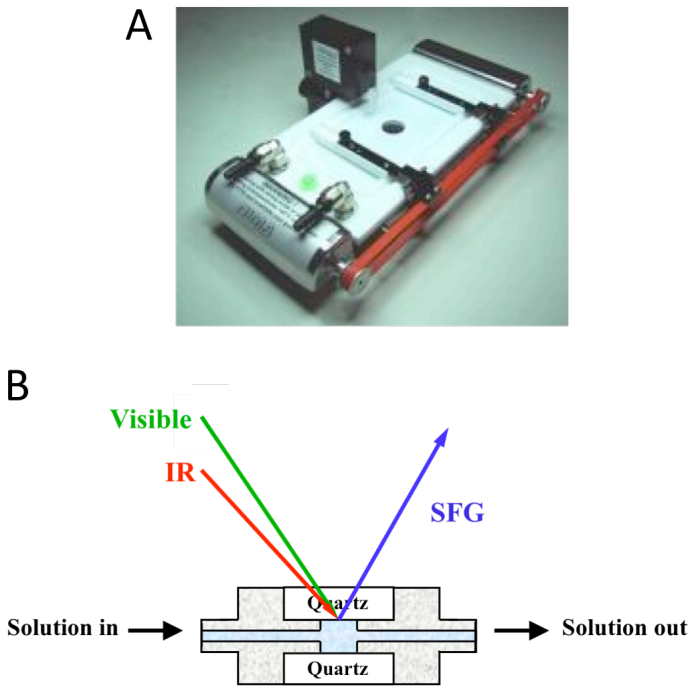

Figure 2.4 Sample holders. A) Langmuir trough for air/water interface experiments. B) Flow cell for experiments at the solid/liquid interface.

To perform VSFS experiments at the solid/liquid interface, quartz and titanium dioxide coated quartz substrates were placed inside a homemade Teflon® flow cell as illustrated in Figure 2.4B. The fabrication of the flow cell has been previously described in detail.[54] The sample area is inside a Plexiglas box, which allows humidity control, and minimizes contamination of samples. The box is purged with nitrogen gas, or dry air in order to enhance the sum frequency signal and minimize infrared adsorption by water in the atmosphere.

The resulting SFG signal was recorded with a photomultiplier tube (Hamamatsu, Japan), which is connected to a gated integrator/boxcar averager (Stanford Research Systems, Inc. Sunnyvale, CA) and computers for data acquisition. All of the data presented in this work was obtained at ssp (s-sum frequency, s-visible, p-infrared) polarization combination and were subject to background subtraction and normalization.

Standards for Alignment Verification

Prior to experiments, alignment was verified by obtaining the nonresonant response from a piece of Z-cut crystalline quartz (Quartz Plus Inc. Brookline, NH) in the full wavelength range as shown in Figure 2.5A. For an optimum alignment, the intensity of the spectrum must be flat over almost the entire wavelength range, although decreasing intensity is expected towards the edges of the spectrum. If the spectrum appears abnormally low in intensity or overly tilted towards either end, the overlap between the 532 nm and the infrared beams must be verified, mainly by fine-tuning the infrared focusing lens near the sample stage. If the spectrum is still not flat, the alignment of optics must be thoroughly verified from all the way from steering optics to detector side, following the pinholes along the path of the beams.

To confirm the wavelength position, a polystyrene film (Thermo Nicolet Corporation, Madison, WI) was used as standard. The film was placed at the OPG/OPA outlet for the infrared beam in order to obtain a quartz spectrum that displays the infrared adsorption peaks for polystyrene, as the one shown in Figure 2.5B. This was compared to the standard spectrum originally included with the LaserVision program, to ensure the peaks occur at the following wavenumbers: 2848 cm^{-1}, 3020 cm^{-1}, and 3056 cm^{-1}. If the

peak positions are off, they can be adjusted by directly changing the positions at the motor 1 controller in the LaserVision computer.

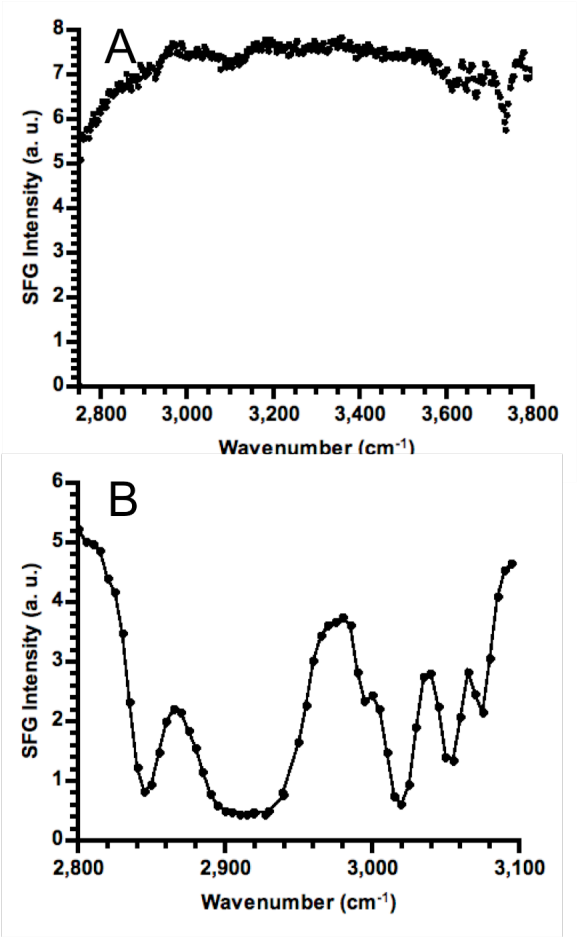

Figure 2.5 Standards for alignment verification. A) Nonresonant response from a square piece of Z-cut crystalline quartz, obtained at a detector sensitivity of 50.0 mV. B) Quartz profile with polystyrene film for infrared adsorption, to confirm wavenumber position.

Once the overall quartz profile and the peak positions are best, the alignment was optimized for the air/water interface. A Langmuir monolayer of eicosanoic acid [$CH_3(CH_2)_{18}COOH$], which is a saturated fatty acid with a 20 carbon long chain and a carboxylic acid headgroup, was used as standard due to the generally high order and stability of the monolayer.

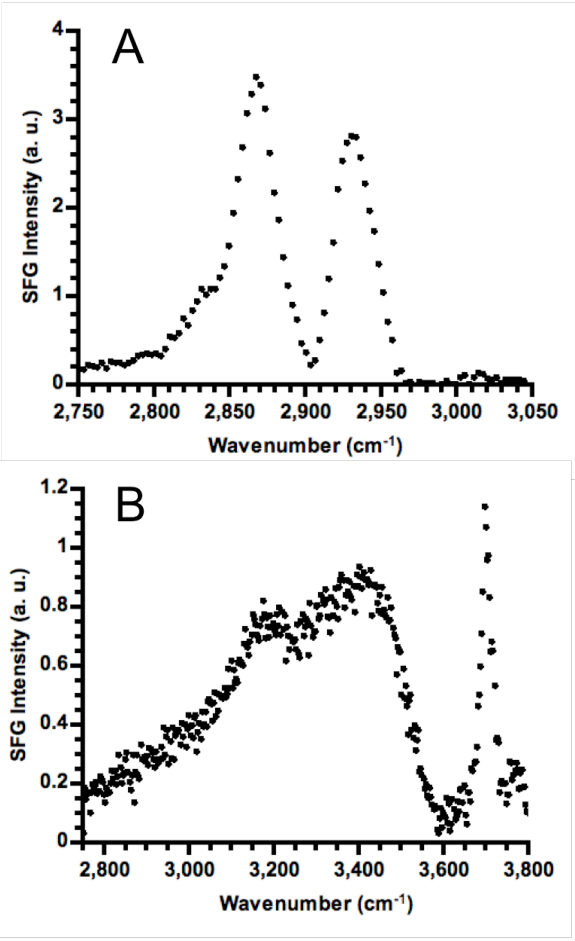

Figure 2.6 Standards for air/water interface alignment. A) Eicosanoic acid Langmuir monolayer with water as subphase, obtained at a detector sensitivity of 50.0 mV. B) Pure water spectrum, obtained at a detector sensitivity of 20.0 mV.

The eicosanoic acid was dissolved in chloroform, and using a micrometer syringe it was added drop wise to the water surface until visually saturated. By real time monitoring of the intensity at 2875 cm^{-1}, which corresponds to the CH_3 symmetric peak, the signal-to-noise ratio was optimized by adjustment of the visible and infrared overlap, mainly by manipulating the focusing lens near the sample stage. The spectrum was obtained for the CH stretch region as demonstrated in Figure 2.6A. The two main peaks show at 2875 cm^{-1} and 2935 cm^{-1}, which correspond to CH_3 symmetric stretch and CH_2 asymmetric. If the intensity of the CH peaks is not satisfactory, further fine-tuning of the infrared focusing lens must be performed. After optimizing the sum frequency signal with the eicosanoic acid standard, a pure water spectrum like the one in Figure 2.7A was obtained to ensure a final optimum alignment.

Water Structure

VSFS has been used to investigate water structure at various interfaces, and it has been found that interfacial water is in general more ordered than bulk liquid and highly sensitive to different properties of the adjacent surface such as hydrophobicity and charged state.[55-57]

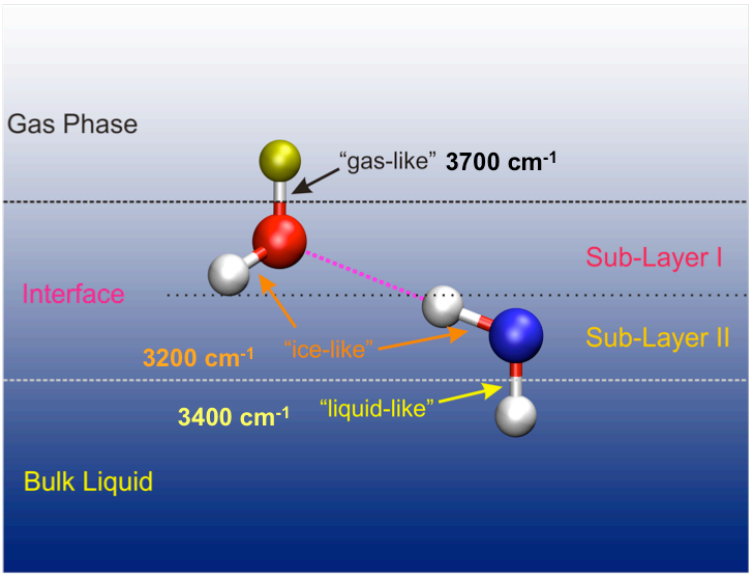

Figure 2.7 Peak assignments for the pure water VSFS spectrum.[60]

As shown in Figure 2.7, the spectrum of pure water features a sharp peak at 3700 cm^{-1}, which it is well known to be non-hydrogen-bonded dangling OH and its frequency is very similar to OH in the gas phase. The region that is hydrogen-bonded features two humps at ~3200 cm^{-1} and ~3450 cm^{-1} that are generally assigned to the ice-like, T_d coordinated water molecules, and liquid-like, more disordered water structures respectively (Figure 2.7).[58,59] These designations arise of the similarities in peak frequencies with the Fourier transform infrared (FTIR) spectra for pure ice and liquid water. It is also believed that the features correspond to water molecules with a more

complete and a less complete hydrogen bonding networks, respectively, although this notion is still a matter of debate.[60]

Water structure is highly sensitive to the charged state of the adjacent surface. For example, at quartz/water and TiO_2/water interfaces, the water structure is significantly altered with changes in the charged state of these oxide surfaces.[52,53,61] Both quartz and TiO_2 surfaces present an acid/base character, and can be protonated or deprotonated as the pH of the solution in contact is lowered or raised. Their isoelectric point corresponds to pH ~ 2.0 and pH ~ 5.5 for quartz and TiO_2, respectively. Therefore, below and above these pH values, the water structure responds to a positively and negatively charged surface, respectively. The intensity in the VSFS signal is therefore larger for more positively charged or more negatively charged surfaces, due to the stronger electric fields available to increase the amount of aligned water molecules.

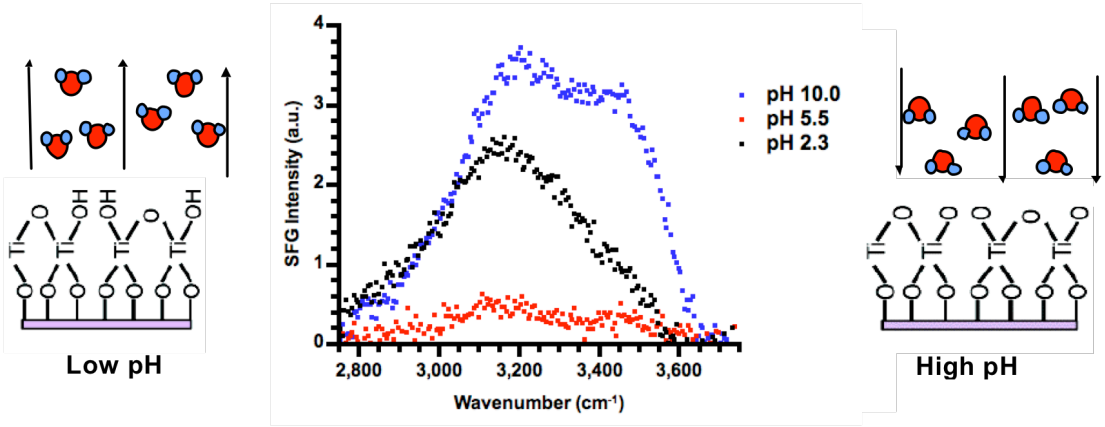

Figure 2.8 Water VSFS spectra of the TiO_2/water interface at various pH values. Effect of surface charged state on water structure.

There is additional evidence that the net orientation of the water molecules changes in response to the electrostatic interactions.[62] If the surface is positively charged, the water molecules are oriented with their hydrogen atoms pointing away from the surface. Similarly, if the pH is raised so that the surface is negatively charged the water molecules orient with their hydrogen atoms towards the surface as depicted in Figure 2.8. As a consequence of this surface property, the VSFS intensity is at its minimum value for water molecules in contact with either quartz or TiO_2 at their isoelectric points. A random orientation of water molecules is expected at the neutral surface.

As it is demonstrated in the following chapters, by analyzing the changes in the overall intensity of the VSFS water spectra, it is possible to get molecular level information about the extent of the interaction between a variety of surfaces and the different ions in solution.

CHAPTER III*

SPECIFIC ANION EFFECTS ON WATER STRUCTURE ADJACENT TO PROTEIN SURFACES

Effects of pH on Proteins

Proteins like bovine serum albumin (BSA) can be adsorbed at the air/water interface and form Gibbs monolayers when in solution.[63] As model protein, BSA contains both negatively [glutamic (Glu) and aspartic (Asp) acids] and positively [lysine (Lys), arginine (Arg), and histidine (His)] charged residues, and its isoelectric point lies near pH 5.0. Similarly to all proteins, the net charge on BSA depends upon the solution pH. Changes in the pH subphase titrate these amino acid residues in the BSA, and the degree of protonation changes the charge density of the protein at the interface.[64-66] VSFS spectra can demonstrate these changes in charge density through the overall intensity of the OH peaks, which in part correspond to the amount of water oriented by the electric fields at the protein/water interface. Figure 3.1 shows the VSFS spectra for BSA Gibbs monolayers at the air/water interface at different pH values. In general, the spectra include both CH and OH vibrational region. At pH 3.0, the protein monolayer should be positively charged, and should orient a significant amount of water molecules at its interface as demonstrated by the prominent OH peaks.

---

* Parts adapted with permission from: Chen, X.; Flores, S. C.; Lim, S. M.; Zhang, Y.; Yang, T.; Kherb, J.; Cremer, P. S. *Langmuir* **2010**, *26*, 16447. Copyright 2010, American Chemical Society.

At pH 5.0, the monolayer is near its isoelectric point; therefore, it is less effective to orient water molecules as manifested by the minimum VSFS intensity in the OH region. As the net charge becomes negative near pH 9.0, the intensity of the OH peaks is enhanced similarly to the low pH case, but in this case the alignment of water molecules is induced by the overall negative charge of the protein.

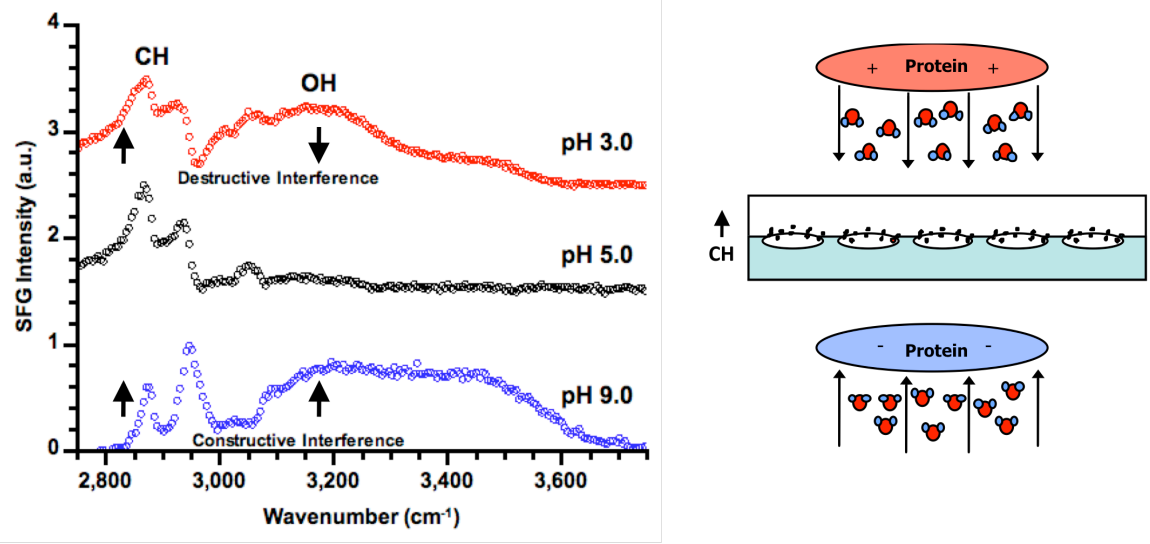

Figure 3.1 VSFS spectra of BSA at various pH values. The spectra demonstrate the effect of surface charge on the intensity of the water peaks. The diagram represents the effect of the protein's net charge on water orientation, and the arrows depict the overall directionality of the CH and OH stretches, which can be confirmed by the interference patterns.

Constructive and destructive interference patterns between the OH and CH stretches, confirm the directionality of the vibrational modes, specially the orientation of the water molecules and their dipole moment (Figure 3.1). For example, hydrophobic moieties like those that contribute to CH stretches are going to be orienting up towards

the air, which can also be seen as hydrophobic. Therefore the directionality of the CH vibrations will be towards the air. If we have a vibration with directionality opposing the CH stretches we will observe a destructive interference pattern, which can be detected as a dip in the spectrum where both CH and OH signals overlap, and indicates that the water molecules are oriented with their H atoms away from the surface. This is exactly the case at pH 3.0, in which the positively charged monolayer induces this orientation. If we have a vibration in the same directionality as the CH stretches, we will observe constructive interference. This is characterized by a slight increase or a rise in intensity where the CH and OH signals overlap, meaning that water molecules are also oriented with their H atoms pointing towards the surface, as it is the case for BSA at pH 9.0 in Figure 3.1.

As BSA forms a charged monolayer, the water molecules at the protein/aqueous interface orient accordingly to the charged state of the surface, and respond accordingly to the anion-protein interaction as it is demonstrated below.

Experimental Methods

Preparation of Salt Solutions

The sodium salts used in this study were Na_2SO_4, NaCl, NaBr, $NaNO_3$, $NaClO_4$, and NaSCN (99+% Sigma-Aldrich Co.), which were used as received without further purification. The solutions were prepared by dissolving the proper amount of salt into deionized water from a NANOpure Ultrapure Water System (18MΩ·cm; Barnstead, Dubuque, IA), to a total concentration of 0.1 M for the protein and ELP experiments. The concentration of $NaSO_4$ was adjusted to 0.033 M to match the ionic strength of the

other solutions. In the case of the surfactants, the solution concentration was 10 mM. In most cases the pH was controlled with HCl or NaOH. For VSFS experiments, a volume of 35 mL of the corresponding sodium salt was used to fill the Langmuir trough.

Preparation of Protein and Surfactant Solutions

The BSA protein (Sigma-Aldrich Co.) was dissolved to prepare a 10 mg/mL stock solution, from which a 250 μL droplet was added to the subphase salt solution already in the trough. The concentrated protein solution was allowed to spread on the surface for 10 minutes for complete monolayer formation. In the case of the protein solutions, the pH was controlled with 5.0 mM phosphate buffer (PBS). The concentration of phosphate ions was relatively low, and constant in every solution, so that the differences observed in the spectra derive particularly from the specific anion effects.

1, 2-Dipalmitoyl-3-trimethylammonium-propane (DPTAP, chloride salt) and 1, 2-dilauroyl-*sn*- glycerol-3-phosphocholine (DLPC) were purchased from Avanti Polar Lipids, Inc. (Alabaster, AL), and sodium 1-dodecanesulfonate (DS) came from Sigma-Aldrich Co. Stock solutions of these amphiphilic molecules were prepared to a concentration of 1 mg/mL in chloroform, from which a 10 μL droplet was spread over the subphase solution. The surface tension was measured with a Wilhelmy plate,[67] and kept constant to 15 mN/m by adjusting the barriers in the Langmuir trough. The ELP was prepared by overexpression in *E.coli* following standard procedures.[38,68,69] The polypeptide was collected after cell lysis via sonication of the cells followed by several inverse phase transition temperature cycling steps for purification. Finally, the polymer

was dialyzed against purified water, lyophilized, and stored at -80 °C until use. Similar to BSA, the ELP was spread on top of the subphase and allowed to equilibrate for 10 minutes to form a complete Gibbs monolayer, with a total ELP concentration of 0.005 mg/mL in solution.

Results

Specific Ion Effects on Water Structure at Protein Surfaces

The VSFS spectra in Figure 3.2 show specific anion effects on BSA monolayers at low, intermediate, and high pH values, which were obtained for the CH and OH region from 2750 cm^{-1} to 3750 cm^{-1}.[66,70,71] Common features were observed in all the spectra regardless of the pH or salt conditions, like a major peak at 2880 cm^{-1}, which can be assigned to the CH_3 symmetric stretch from the hydrophobic residues on the protein. The CH_2 symmetric stretch manifests weakly at 2840 cm^{-1}, and at 2950 cm^{-1} a combination of Fermi resonance and CH_3 asymmetric stretch can be found. Other common features are the small peaks at 2915 cm^{-1} and 3050 cm^{-1}, which correspond to CH_2 stretch (most likely from isopropyl groups in valine or isoleucine residues), and aromatic CH stretch (possibly from phenylalanine), respectively. The partial reordering of the hydrophobic moieties up towards the air gives rise to these features, which remain unaltered as the solution conditions are changed. This has been demonstrated by conducting similar experiments in pure D_2O, instead of H_2O.[66,70,71] Additionally, the spectra share two common features in the OH region, at 3200 cm^{-1} and 3450 cm^{-1}, which correspond to “ice-like” and “liquid-like” interfacial water structures as has been previously described.

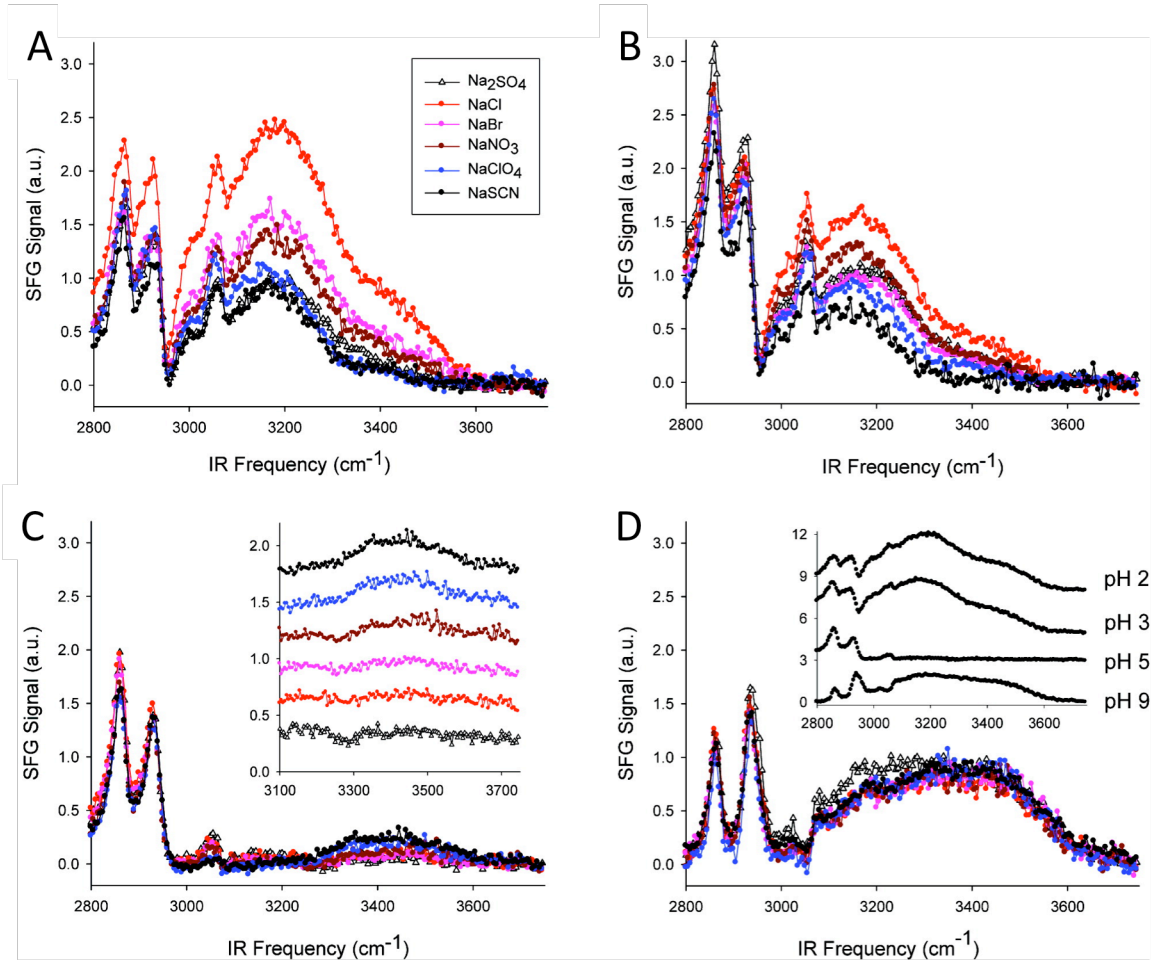

Figure 3.2 Specific anion effects on BSA at various pH values. A) An inverted Hofmeister series at pH 2.0; and B) pH 3.0. C) A direct Hofmeister series at pI of BSA (pH 5.0). Offset to avoid crowding. The inset shows a closer view of the OH stretch region. The effects are very weak as compared with PNIPAM results.[11] D) Virtually, no Hofmeister effects at pH 9.0. The inset shows control experiments for BSA without additional salts under the different pH conditions chosen in this study.

The specific anion effects are particularly pronounced at pH 2.0, and at pH 3.0 they are similar but weaker due to the weaker net positive charge of the protein (Figures

3.2A and 3.2B). In the presence of a dominant positive charge, the surface is partially neutralized due to the anion-BSA interactions. In this case larger and more polarizable anions that tend to be weakly hydrated,[72] like SCN^- and ClO_4^-, preferentially bind to neutralize the surface and the more chaotropic the anion is, the more effective it will lower the absolute value of the surface charge. This manifests as weaker VSFS intensity for the black and blue curves in Figures 3.2A and 3.2B. On the other hand, smaller anions like Cl^-, which are better solvated and remain more easily in the bulk solution, interact the least effectively with the positively charged surface, therefore neutralizing to a lesser extent the positive charge of the protein. For that reason, the VSFS intensity for anions like Cl^- (red curve in Figures 3.2A and 3.2B) is the most prominent after the introduction of the salt, because more positive electric fields remain available to orient water molecules at the protein/aqueous interface. Therefore at low pH, due to neutralization of the surface charge, there is an apparent inverted Hofmeister series observed through the water signal, still the anion-macromolecule interaction follows the direct Hofmeister trend as will be further demonstrated in Chapter IV.

In Figure 3.2C, the VSFS spectra of neutral BSA solution at the air/water interface demonstrates a similar but much less obvious anion effect than that observed previously in presence of neutral PNIPAM.[27] In this case, both the water structure and the anion-PNIPAM interaction follows a direct Hofmeister series, and the anion-BSA interaction at pI 5.0 shows this effect as well. Basically SCN^-, and ClO_4^- interact the most with the neutral macromolecules, followed by NO_3^-, Br^-, Cl^-, and SO_4^{2-}. As shown in from Figure 3.2C, the more chaotrope anions like SCN^- charge negatively the BSA

surface to a greater extent, and in turn generate a more intense VSFS signal in the water region, as compared to less chaotropic anions.

When BSA is negatively charged at high pH, the surface potential is sufficiently negative to virtually repel anions from the interface. Water ordering appears to be independent on the presence of anions. There are virtually no specific anion effects in the VSFS water signal as demonstrated by the similarity in spectra for the different salt solutions in Figure 3.2D. However, some weaker anion interactions might be present via counter ion mediated interactions just about a monolayer or two in the protein/aqueous interface, and might be observed at much lower concentratios.[73]

As shown in Figure 3.2A, sulfate ion (black curve with triangle), which generally is a kosmotropic anion in the Hofmeister series, behaves more chaotropic as the charge of the protein becomes more positive. This abnormal behavior can be explained in terms of electrostatic interactions, which are stronger for sulfate ion due to its double charge, as compared to the other monovalent anions. Therefore, sulfate ions participate in stronger charge-charge interactions, and once adsorbed to the surface it is doubly effective at neutralizing the net positive charge. Its effect is comparable to that of SCN^- or ClO_4^-.

Specific Ion Effects on Water Structure at Charged Surfactant Surfaces

The previous observations on protein surfaces are valid for surfactant monolayers as well. Comparable to BSA, and as demonstrated in Figures 3.3A to 3.3C, different anions affect similarly the water spectra when amphiphilic molecules form charged

Langmuir monolayers on water surfaces. It is important to note that none of the charges on these three molecules are titratable under the conditions of these experiments.

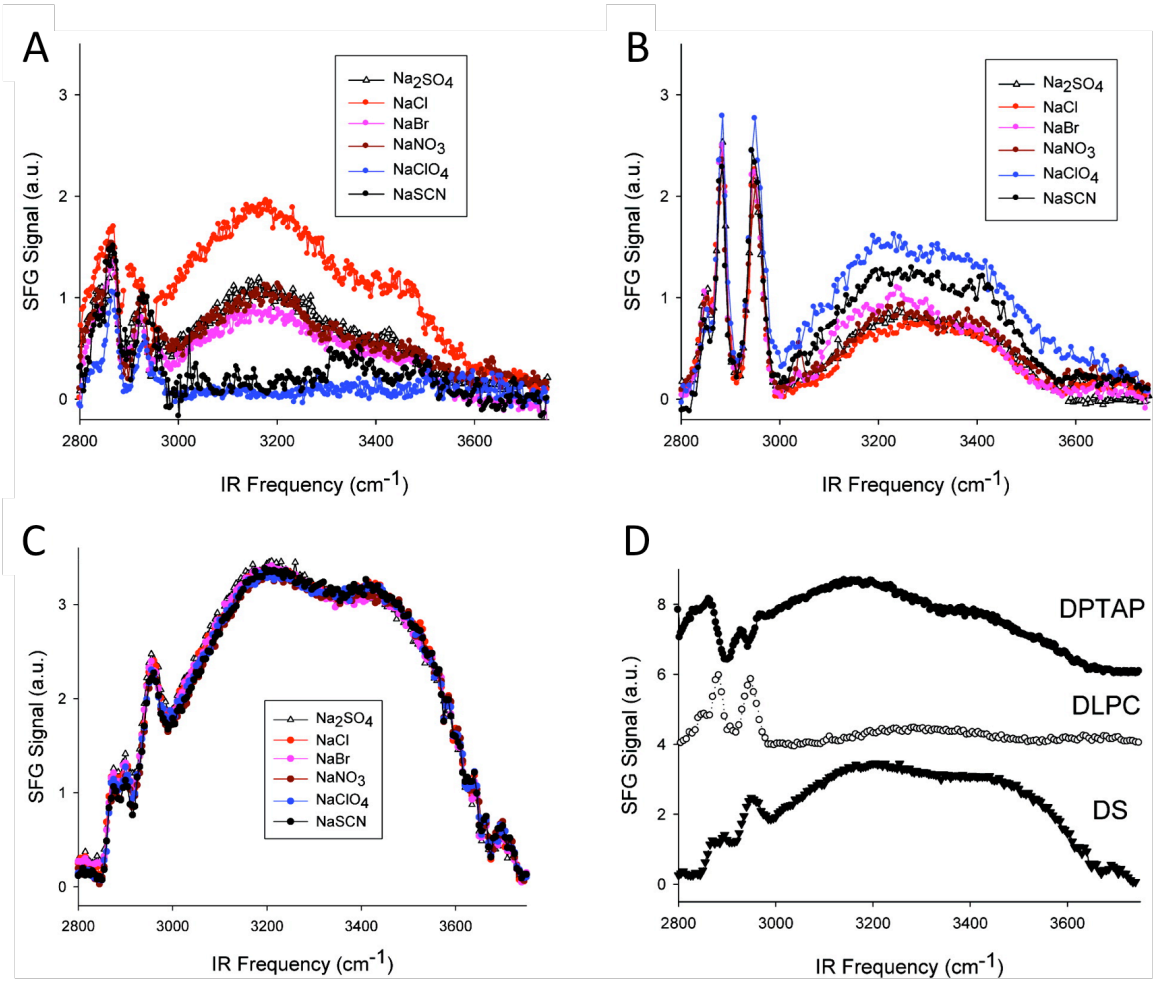

Figure 3.3 Specific anion effects on surfactant monolayers. A) A DPTAP monolayer or a positively charged surfactant. B) A DLPC monolayer or neutral lipid; and C) a DS monolayer or negatively charged surfactant. D) Control experiments with the amphiphilic molecules in the absence of salts. Data offset for clarity.

All spectra contain two groups of peaks in the CH region at 2880 cm^{-1} and 2950 cm^{-1}, which arise from the CH_3 symmetric stretch and CH_2 symmetric stretch, and the Fermi resonance and CH_3 asymmetric stretch. Similar to the OH region in the BSA spectra, the net charge on the monolayers induces a significant amount of water structure both at the positive and negatively charged surfactant monolayers as demonstrated by Figure 3.3D.

Figure 3.3A shows the results for a positively charged surfactant, DPTAP, for which the specific anion effects are similar to those observed on the positively charged BSA. An overall inverse Hofmeister effect on the water structure is measured. The results in Figure 3.3B for the neutral lipid, DLPC, demonstrate similar effects to those observed in neutral BSA, and PNIPAM. A direct Hofmeister series is observed in the water structure, and the effects on DLPC are more pronounced than in BSA. When spreading the negatively charged surfactant, DS, on the surface, the spectra display virtually no specific anion effects. The results with the charged surfactants are consistent with the notion that the interactions are dictated by the net charge of the anions and the monolayers, and not exactly by their chemical specificity.

Specific Ion Effects on Water Structure at a Neutral Polypeptide

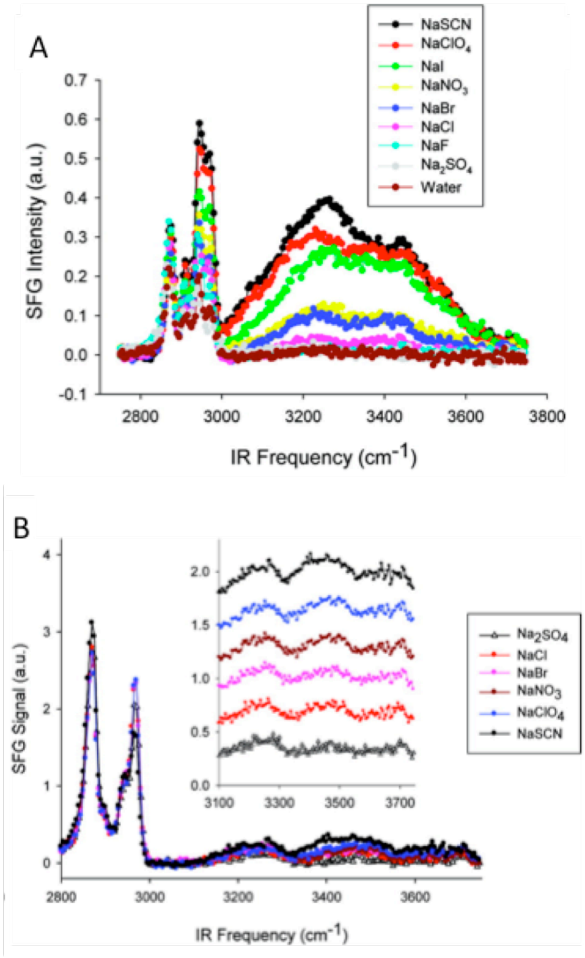

Figure 3.4 Specific anion effects on neutral polypeptides. A) Neutral PNIPAM,[27] and B) ELP Gibbs monolayers adsorbed at the air/water interface. Data offset and magnified for clarity.

VSFS spectra were taken for a neutral ELP in order to confirm if a weak direct Hofmeister series was a general phenomenon for neutral polypeptides. To obtain a more clear view, we investigated the effect of having exposed versus buried NH moieties in

our macromolecules, since the NH moieties in the amide groups are the putative binding sites for anions.[74] For example, in the case of PNIPAM in which the amide groups are present in the side chains rather than the backbone, the specific anion effects are more prominent (Figure 3.4A).[27] Then, it is expected that for the neutral BSA in which the amide groups are part of the backbone, the NH moieties are relatively inaccessible to direct interactions with chaotropic anions. This would manifest as the weaker effect on the water structure at the protein/aqueous interface as demonstrated in Figure 3.2C. Similarly, the neutral ELP $(Val\text{-}Pro\text{-}Gly\text{-}Val\text{-}Gly)_{120}$ has its amide moieties as part of the backbone, and it is expected to have weaker anion effects as well.

The results for Gibbs monolayers of a neutral ELP in presence of the different anions are shown in Figure 3.4B. The spectra is characterized by four peaks in the CH region at 2880 cm^{-1} (CH_3 symmetric stretch), 2915 cm^{-1} (CH stretch), 2940 cm^{-1} (Fermi resonance), and 2980 cm^{-1} (CH_3 asymmetric stretch). The OH region presents the resonances at 3200 cm^{-1} and 3400 cm^{-1}, which are visibly weak even in the presence of the most chaotropic anions. These observations are strikingly similar to the neutral BSA monolayers, confirming the notion that weaker anion binding occurs for NH moieties that are part of the backbone rather than the side chains. Still, a direct Hofmeister effect is observed for the neutral ELP, weaker, but similar to PNIPAM (Figures 3.4A and 3.4B). These results are in agreement with previous inverse phase transition measurements of PNIPAM and ELP in bulk aqueous solutions, which also demonstrate that anions bind more strongly to PNIPAM than to neutral ELPs.[28,38]

Discussion

From the results presented, it can be observed that the net charge of the surface is the dominant factor that determines a system's interfacial water structure and overall salt effects, rather than the specific surface chemistry. Basically, neutral surfaces display moderate anion effects, following a direct Hofmeister effect on water structure, in which chaotropic anions like SCN^- and ClO_4^- preferentially accumulate, and generate a more intense water spectra. Positively charged surfaces induce grater specific anion effects that follow an inverse Hofmeister series, and increasing the net positive charge makes those effects appear stronger. Basically, at a positively charged surface it is the kosmotropes like Cl^- the ion, which cause the most intense water signal. However, on negatively charged surfaces there are virtually no specific anion effects. In general, these effects on water structure can be understood in terms of the preferential adsorption of the more chaotropic anions.

Previous VSFS studies have demonstrated that the water peaks are mostly generated by the local electric fields at the surface, which align the interfacial water molecules.[56,75,76] When ions adsorb at an interface, the surface potential is altered, and the adsorption can be viewed as the equilibrium of ion partitioning between the bulk solution and the interfacial layer. Therefore, if there is an overall attractive interaction between the ion and the surface, then the ion will accumulate at the surface until it is balanced by the electrochemical potential. The equilibrium partitioning depends on the binding strength, the bulk ion concentration, and the charge density of the surface. The effects of ion adsorption on surface potential can be modeled with a modified version of

the Gouy-Chapman-Stern theory, as has been demonstrated for initially uncharged systems.[12] In this work, we extend this model to apply to systems, which are initially charged, either positive or negative.

According to the Stern model, ion adsorption can be described by a Langmuir model with an electrostatic term,[67]

$$\sigma_{adsorption} = \frac{zeN_S \frac{C}{K_D} \exp\frac{ze\varphi(0)}{kT}}{1 + \frac{C}{K_D} \exp\frac{ze\varphi(0)}{kT}} \qquad (1)$$

where $\sigma_{adsorption}$ is the surface charge density of adsorbed ions, z is the valence of the ions, C is the bulk ion concentration, K_D is the equilibrium dissociation constant, and N_S is the number density of the binding sites. The exponential term represents the electrochemical potential, where $\varphi(0)$ is the surface potential, and kT the thermal energy. However, this equation is not directly useful, since both $\sigma_{adsorption}$ and $\varphi(0)$ are unknown.

The Gouy-Chapman theory describes the overall charge density in the diffuse double layer that is induced at a charged plane contacting an electrolyte solution.[67] The diffuse double layer carries a net charge of opposing sign to that of the charged plane, and it is defined by the following equation,

$$\sigma_{diffuse} = -(8I\varepsilon_r\varepsilon_0 kT)^{1/2} \sinh\frac{ze\varphi(0)}{2kT} \qquad (2)$$

where $\sigma_{diffuse}$ is the net charge density, I is the ionic strength, ε_r is the dielectric constant, and ε_0 is the permittivity of vacuum.

Then, the following equation has to be satisfied in order to ensure electric neutrality,

$$\sigma_{diffuse} + \sigma_{adsorption} + \sigma_{plane} = 0 \qquad (3)$$

where σ_{plane} is the surface charge density in the absence of ion adsorption. With the three unknowns, $\sigma_{adsorption,}$ $\sigma_{diffuse}$, and $\varphi(0)$, and three equations, we can obtain a solution for the surface potential that is sensitive to σ_{plane} as well as K_D.

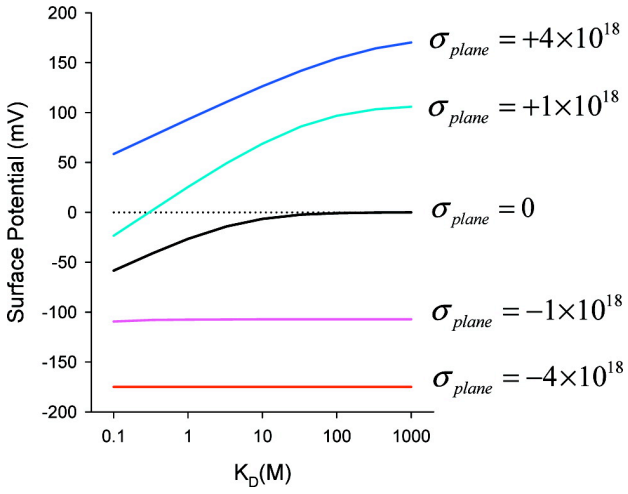

Figure 3.5 Gouy-Chapman-Stern model. The surface potential results for anion adsorption at various σ_{plane} (m^{-2}) values as a function of K_D. The variables C and N_S were set at 100 mM and 5 x 10^{18} m^{-2}, respectively, and the anion and its counterion were assumed to be monovalent. The red (bottom) and the blue (top) curves represent limiting cases of very high negative and very high positive charge density, respectively.

The specific anion effects on the intensity of the water peaks can be modeled as a surface potential dependence on K_D, which is the only ion specific term in the equations. Figure 3.5 demonstrates examples of variation of surface potential with K_D. For example, the black curve represents the surface potential dependence on K_D for an initially uncharged system (σ_{plane} = 0), which is basically monotonic, and anions that bind more tightly or have a smaller K_D yield a more negative surface potential. The slope of the curve represents the sensitivity of the surface potential to K_D, which in turn represents the magnitude of the specific ion effects on interfacial water alignment. When binding is weak (K_D > 10 M), the curve is virtually flat, but as the binding strength increases, the slope becomes steeper. The results agree with our observation that only more chaotropic anions bind strongly, rather than less chaotropic species like Cl^-.

Anion adsorption to neutral BSA and ELP is relatively weak (Figures 3.2C and 3.4B), if compared to PNIPAM (Figure 3.4A). When ions interact with pendent amide moieties as in the case of PNIPAM, the apparent dissociation constants were demonstrated to be in the range of 0.15 M - 15 M, from which the smallest K_D values correspond to the more chaotropic anions.[27] Based on the model provided, the dissociation constants should be ≥ 20 M for the neutral protein and the polypeptide, due to the relative inaccessibility of the amide moieties in the backbone. However, for charged surfaces, the specific anion effects will depend greatly on the sign and magnitude of σ_{plane}. Figure 3.5 also shows the changes in surface potential for surfaces with two positive and two negative σ_{plane} values. The curves become steeper for a more positively charged surface. Even ions that bind moderately weakly (larger K_D values),

can be distinguished from those that bind very weakly. In contrast, for negatively charged surfaces, the curves are nearly flat even at 100 mM, indicating little to no adsorption of ions. The results with this model are in very good agreement with the experimental observations of the various BSA and surfactant surfaces in Figures 3.2 and 3.3.

Conclusion

In general, we found that the interfacial water structure can follow either a direct or an inverted Hofmeister series, which depends on the charge state of the interfacial layer. The interfacial water ordering is a pure consequence of the direct anion/macromolecule interactions, which are dominated by the overall surface charge density, and at the same time dictated by a few basic physical properties on ions. The observations are similar for various systems like proteins with different charge, and surfactants with various charged head groups, proving that it is a general phenomenon based on electrostatics rather than a mechanism depending on a particular surface chemistry. Therefore, the most of the analysis above may be extended beyond simple inorganic ions as well.

CHAPTER IV

INTERACTIONS OF ANIONS WITH NEGATIVE AND POSITIVELY CHARGED SURFACES FOLLOWS A DIRECT HOFMEISTER SERIES

In the present Chapter we investigate the effect of the Hofmeister anions on quartz and TiO_2, which are used as model negative and positively charged hydrophilic surfaces, in order to understand the interaction of anions with interfaces where surface charge is one of the main factors dominating the phenomenon. We also investigated the effects of anions on octadecyltrichlorosilane (OTS) covered quartz, and lysozyme Gibbs monolayers, which are representative of hydrophilic surfaces with certain hydrophobic character, bearing negative and positive charge respectively. From the results of our experiments, it is evident that the order of the interactions of anions with various types of surfaces with different charge sing and degree of hydrophilicity follows a direct Hofmeister series. We demonstrate that adsorption of anions to aqueous interfaces is favored for chaotropic anions, regardless of changes in sign or degree of hydrophilicity of the surfaces.

Experimental

Preparation of Negatively Charged Surfaces

IR grade quartz discs (1" diameter by $\frac{1}{8}$" thick; Quartz Plus Inc. Brookline, NH) were cleaned by following standard procedures.[61] In brief, the quartz discs were

immersed in piranha solution, followed by oven calcination, and subsequent immersion in concentrated sulfuric acid to obtain a hydroxylated surface.

Cleaned quartz discs were used as substrates for the preparation of negatively charged hydrophobic surfaces, which consisted on the self-assembly of octadecyltrichlorosilane or OTS (95%, Acros Organics) monolayer. Prior to the monolayer preparation, the cleaned quartz discs were immersed in a 2 M NaOH solution, followed by rinsing with copious amounts of deionized water, and drying completely at 130°C. A 0.1% OTS solution was prepared in hexane, and the dry quartz pieces were immersed in this solution for 2 hours to form the OTS monolayer. Final rinsing with water, and sonication in ethanol/water mixture ensured the removal of residual OTS.[77]

Preparation of Positively Charged Surfaces

The cleaned quartz discs were used as substrates to grow TiO_2 thin films, which were prepared by evaporating titanium (IV) isopropoxide (97% $Ti(O\textit{i}Pr)_4$, Aldrich, Milwaukee, WI) for 10 minutes to allow it to react with the surface silanol groups. Finally, oven calcination was employed at 500 °C in order to oxidize the organic precursor into a few layers of TiO_2, which were suitable for the VSFS experiments.

The lysozyme protein (Sigma-Aldrich Co.) solutions were prepared by dissolving the proper amount of solid in deionized water to obtain a 10 mg/mL solution. At this concentration, and due to the presence of positively charged amino acid residues, the lysozyme solutions had a pH ~ 4.5, at which measurements were taken.

Characterization of TiO_2 Thin Films

The TiO_2 films were previously characterized in our laboratory by x-ray photoelectron spectroscopy (XPS), atomic force microscopy (AFM), and ellipsometry in order to elucidate the elemental composition, roughness, and thickness of the films.[61] Similar measurements were reproduced for the samples used in this study in order to confirm the presence and properties of the TiO_2 thin film.

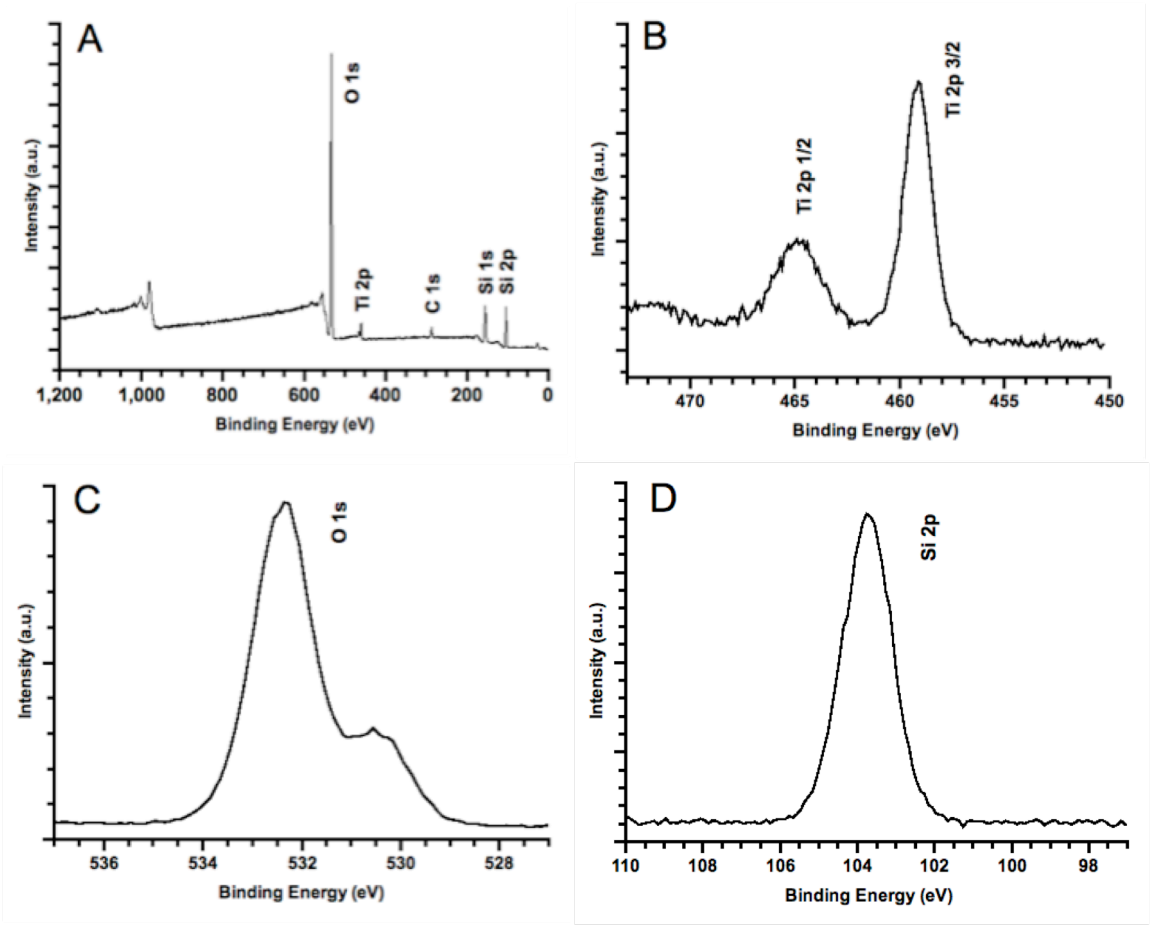

Figure 4.1 X-ray photoelectron spectroscopy for the TiO_2 thin film. Results for: A) survey scan; B) HR scan for Ti 2p region; C) HR for O 1s, and D) HR for Si 2p.

A Kratos Axis Ultra Imaging X-ray photoelectron spectrometer (XPS or ESCA for electron spectroscopy for chemical analysis) was utilized to confirm the chemical composition of the thin films on the quartz pieces. Figure 4.1A shows the survey scan, which was obtained from 1100 eV to 0 eV at a pass energy 80/160, and higher resolution (HR) scans for the Ti 2p, O 1s, and Si 2p regions were obtained at a pass energy 20/40 as demonstrated in Figures 4.1B to 4.1D. The data was used to confirm the presence of TiO_2, as characterized by the presence of the two peaks at 459.0 eV and 465.0 eV, which correspond to $2p_{3/2}$ and $2p_{1/2}$ respectively (Figure 4.1B). No Ti metal peaks were observed at 453.0 eV, meaning that most of the $Ti(O\textit{i}Pr)_4$ precursor was converted into TiO_2 during calcination. There were no obvious shoulders at 457.0 eV and 462.5 eV that would indicate the presence of TiO species. Similarly, there were no peaks at 458.2 and 463.7 eV, which are indicators of Ti_2O_3 species. For the thin films, the difference in binding energy between the O 1s peak at 532.35 eV (Figure 4.1C) and the Ti $2p_{3/2}$ at 459.0 eV [ΔBE (O1s-Ti$2p_{3/2}$)] is in agreement with literature values ~ 71.5±0.2 eV, which corresponds to TiO_2 species.[78,79] The ΔBE (Ti$2p_{3/2}$-Ti$2p_{1/2}$) values are ~ 5.8 eV, which accounts for presence of Ti^{+4} species. The ΔBE (Ti$2p_{3/2}$-Si2p), for which Si 2p is located at 103.5 eV (Figure 4.1D) corresponds to values near ~ 355.4±0.2 eV that denote the Ti 2p species are in the overlayer and the Si 2p species in the substrate.

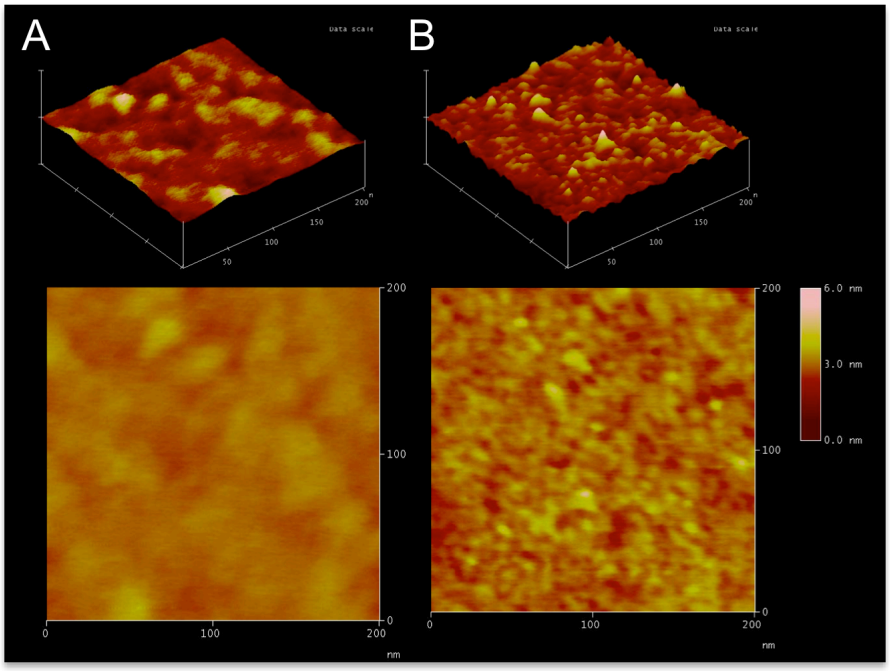

Figure 4.2 Atomic force microscopy characterization of the solid surfaces. Results for: (A) quartz surface after cleaning procedure (RMS 0.074), and B) TiO_2 covered quartz surface, after 10 minutes exposure to precursor and calcination (RMS 0.242, grain height 0.715).

Tapping mode atomic force microscopy (AFM) images were obtained with a MultiMode^{TM} scanning probe microscope (MM-SPM), for which the quartz pieces and TiO_2 covered samples where cut down to a size of 9.0 x 9.0 mm in order to fit the sample area of the microscope. Figure 4.2 shows the AFM images obtained with a scanner of the type E, which allowed acquiring images with subnanometer resolution. The image in Figure 4.2B shows grain heights ~0.715 nm that are present in the quartz

surfaces that were exposed for 10 minutes to the Ti(O*i*Pr)$_4$ precursor, and which are not present in the topography of bare quartz pieces.

It should be noted that the TiO_2 thin films generated in the way could be classified as neither anatase nor rutile, but rather as an amorphous combination of the two. VSFS was used to further characterize the films in contact with aqueous solution. The presence of an isoelectric point near pH 5.5 can be demonstrated by a minimum in the VSFS water structure at that pH value (Figure 4.3).

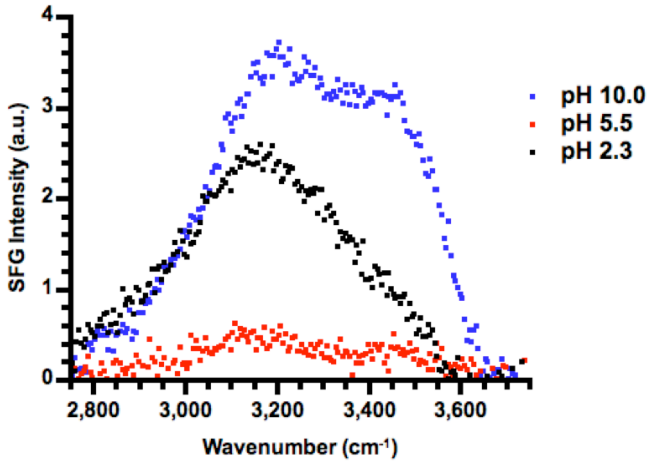

Figure 4.3 The VSFS water spectra for TiO_2 surfaces at various pH values. The spectra demonstrate the isoelectric point of the oxide thin film at approximately pH 5.5.

At pH 10.0, the water molecules should orient with their hydrogen atoms facing toward the negatively charged surface. Their orientation inverts as the pH is tuned below pH 5.5 because the surface becomes positively charged.

Preparation of Salt Solutions

Salt solutions were prepared in deionized water obtained from a Millipore filtration system (18MΩ·cm; NANOpure Ultrapure Water System, Barnstead, Dubuque, IA). High purity inorganic salts were dissolved to have a 0.10 M stock solution of each NaSCN, $NaClO_4$, $NaNO_3$, NaBr, and NaCl (99+% Sigma-Aldrich Co.). The low concentration salt solutions used in the actual experiments were prepared by further diluting the stock solutions to have 0.10 mM – 10.00 mM solutions. Micromolar salt concentrations are enough to perturb the water structure at the solid/liquid interface,[80] and essential to observe the differences between the effects of the various anions avoiding significant signal screening. The actual concentration of Na_2SO_4 was one third of the chosen concentrations in order to match the ionic strength of the monovalent salts. The pH of the solutions was adjusted by using NaOH or HCl to reach pH 10.0 or pH 2.0 respectively. The pH 10.0 is well above the pH values for the isoelectric points of quartz and TiO_2 surfaces.[61,81] It was chosen to maximize the amount of deprotonated OH surface groups, and increase the negative charge of the surfaces. The pH 2.0 was chosen to deprotonate the OH groups on the hydrophilic TiO_2 surface, and increase the overall positive charge of the surface.

In our solutions there is always a background amount of sodium counterion from NaOH, which mediates the adsorption of anions. Similarly, at low pH, there is a background amount of chloride, which is a kosmotropic anion that does not compete as much with chaotropic anions for adsorption. Therefore, any differences observed in VSFS water spectra are purely due to the effects of the anions.

Results and Discussion

Interactions of Hofmeister Anions with Negatively Charged Surfaces

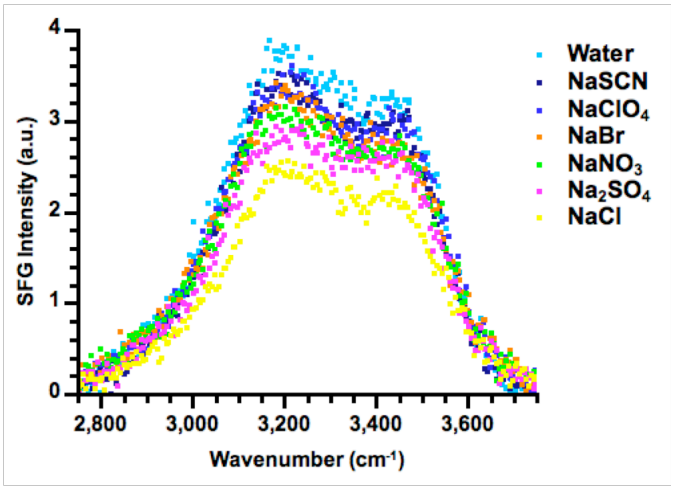

Figure 4.4 Quartz surfaces at pH 10.0 in contact with 0.10 mM sodium salts. The results display a direct Hofmeister effect. The concentration for Na_2SO_4 is 0.033 mM.

The VSFS water spectra for a quartz surface in contact with pH 10.0 sodium salt solutions are shown in Figure 4.4. The spectra are dominated by the presence of two OH stretches at 3200 and 3450 cm^{-1}, which correspond to tetrahedraly coordinated water structure, and less ordered water.[53] The pure water solution gives rise to the highest SFVS intensity from the spectra. Addition of sodium salts reduces the amount of VSFS signal due to charge screening effects, which are minimized when using micromolar salt concentrations. This was observed for the various solid/liquid interfaces used in this study. The intensity for the water spectra at this interface in presence of salts follows a

direct Hofmeister series. The most chaotropic anions like SCN^- and ClO_4^- adsorb preferentially to the solid surface, possibly through a counter ion (Na^+) mediated interaction. The series is completed by Br^-, NO_3^-, SO_4^{2-}, and Cl^-. In cases like quartz in which the surface is purely hydrophilic and negatively charged, divalent kosmotropic anions like SO_4^{2-} behave slightly more chaotropic. Therefore, SO_4^{2-} adsorbs better than Cl^- to the surface, contributing to an overall higher negative charge, and a more intense VSFS spectra.

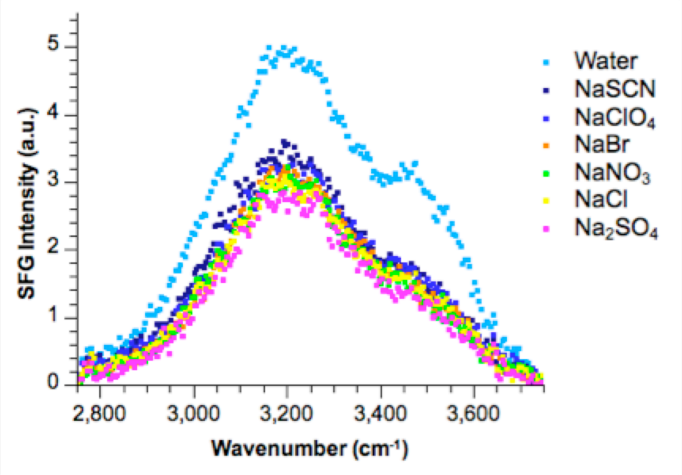

Figure 4.5 TiO_2 surfaces at pH 10.0 in contact with 0.1 mM sodium salts. The data displays a direct Hofmeister effect. The effects are less obvious than with the quartz surface.

The results with quartz surfaces were confirmed by using negatively charged titanium dioxide (TiO_2) surfaces as demonstrated in Figure 4.5. Even if the anion effects

are weaker, it is clear that for a sufficiently high negatively charged surface, the specific anion effects follow a direct Hofmeister order of interaction.

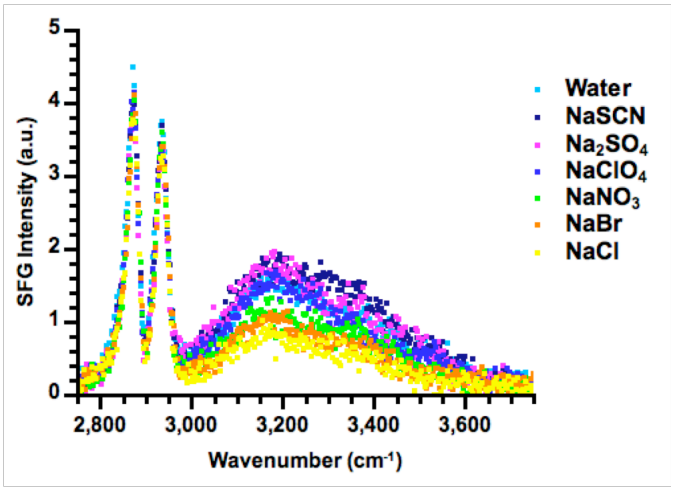

Figure 4.6 OTS-covered quartz surfaces in presence of anions. The spectra at pH 10.0 in contact with 0.10 mM sodium salt solutions display a direct Hofmeister effect.

In Figure 4.6, the VSFS water spectra for OTS covered surfaces in presence of sodium salts are shown. The spectra is dominated by the presence of two main CH stretches at 2875 cm^{-1} and 2940 cm^{-1}, which correspond to CH_3 symmetric stretch and Fermi resonance from the hydrophobic self assembled monolayer. In the OH stretch region the two main water peaks are present at 3180 and 3400 cm^{-1}. Increasing pH of the solution can enhance the intensity of the peaks; at the molecular level, formation of the OTS monolayer is imperfect and does not cover all the available silanol groups, which can still be deprotonated.[82] The pure water spectrum at pH 10.0 is less intense as that of pure quartz because of the presence of OTS, and it can be observed that the addition of

chaotropic anions like SCN^- and ClO_4^- similarly charge to some extent the hydrophobic interface and increase the overall intensity of the corresponding water spectra. The behavior of SO_4^{2-} is even more chaotropic than in the case of pure quartz (Figure 4.4) and its spectrum intensity is similar to that of SCN^- or ClO_4^-. The intensity of the spectra decreases as less chaotropic anions are introduced, and the overall order of the effects follows a Hofmeister series: SCN^-, SO_4^{2-}, ClO_4^-, NO_3^-, Br^-, and Cl^- interacting the least with the surface. The interaction is possibly mediated by Na^+ ions, similarly as in the case of pure quartz, and in magnitude the intensities are very similar as well.

In the case of the salts used in this study, we observe that as Na^+ ions interact predominantly with the negatively charged surface, the VSFS signal is reduced significantly by charge screening effects. Cl^- ion is considered to be the dividing line between chaotropes and kosmotropes and one of the least chaotropic anions used in this study. Due to its nature, there is probably just a very small (little to none) contribution from Cl^- to the overall negative surface charge that induces the VSFS water signal alignment. In contrast to more chaotropic anions, Cl^- is strongly hydrated, and remains better solvated in the bulk of the solution as depicted in Figure 4.7. On the other hand, the most chaotropic anions used in this study, SCN^- and ClO_4^-, which are generally larger and less solvated are charging the solid/liquid interface much more effectively. These results agree with the accepted notion that chaotropes have a higher propensity for interfaces,[36] and the results demonstrate that changing the degree of hydrophilicity of the surface by going from pure quartz to OTS-covered quartz does not change the order in which anions interact with the different surfaces.

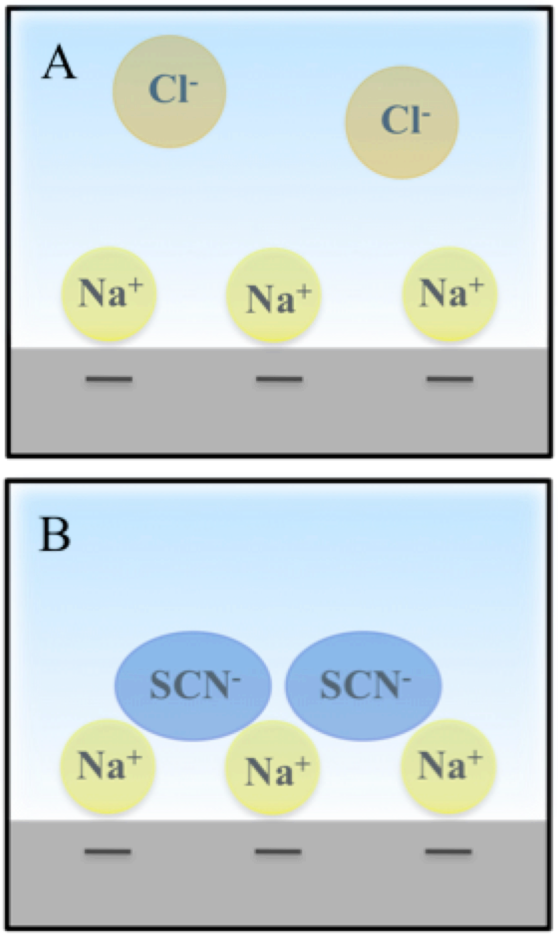

Figure 4.7 Ion adsorption to a negatively charged surface. A) The counter ion Na^+ adsorbs to the surface and quench the VSFS signal; Cl^- prefers to stay in solution and contributes the least to the alignment of water molecules at the interface. B) Larger anions like SCN^- or ClO_4^- adsorb preferentially to the quartz surface therefore enhancing the VSFS water signal, as compared to Cl^-.

Additionally, the effect of SO_4^{2-} as a more chaotropic anion in Figure 4.6 is in agreement with previous studies where salt effects have been analyzed for polar surfaces

using a solute-partitioning model (SPM).[47,83] In these cases, for polar amide surfaces, SO_4^{2-} shows very similar effect as SCN^- and ClO_4^-, which compares to our results with OTS covered surfaces, which even if it is mostly a hydrophobic monolayer, still holds a negative charge and a certain degree of hydrophilicity at the molecular level.

Interestingly, these observations are valid only at micromolar concentrations, and the effects of anions banish as the salt concentration increases and the surface charge is significantly screened. In previous studies, we have demonstrated that anions do not alter VSFS water structure at negatively charged BSA protein aqueous interface.[56] This might not exactly occur because of repulsion of anions by the negatively charged surface, but it might happen because anions do not interact that strongly with a surface that has been significantly neutralized by Na^+ ions from the relatively higher concentration solution. Indeed, control experiments at higher concentration salt solutions do not show significant differences amongst anions in neither quartz nor OTS covered surfaces.

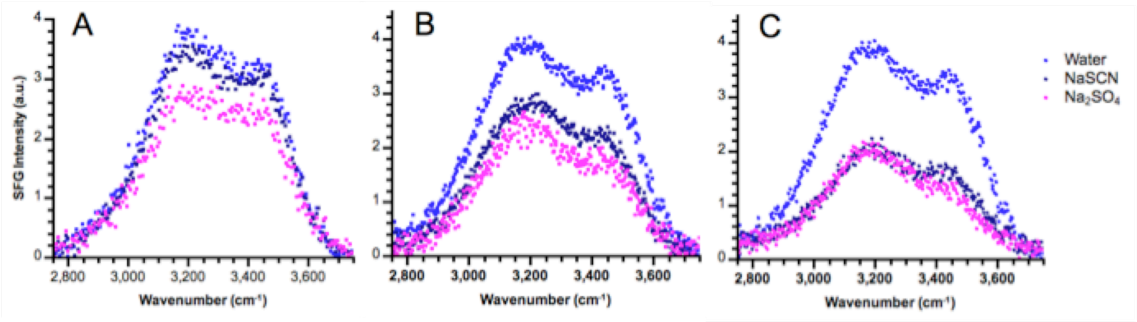

Figure 4.8 Quartz surfaces at pH 10.0 in contact with various sodium salt solutions. At A) 0.1 mM, B) 10 mM, and C) 100 mM Na^+ salt solutions, the effects are less obvious as the salt concentration increases.

For example, the quartz surfaces from Figures 4.8A to 4.8C demonstrate that as the amount of salt added in solution decreases, signal quenching occurs to a less extent, and the differences between the effects of anions on the VSFS water spectra are enhanced. This was observed as well with OTS monolayers at higher salt concentrations, as shown in Figure 4.9.

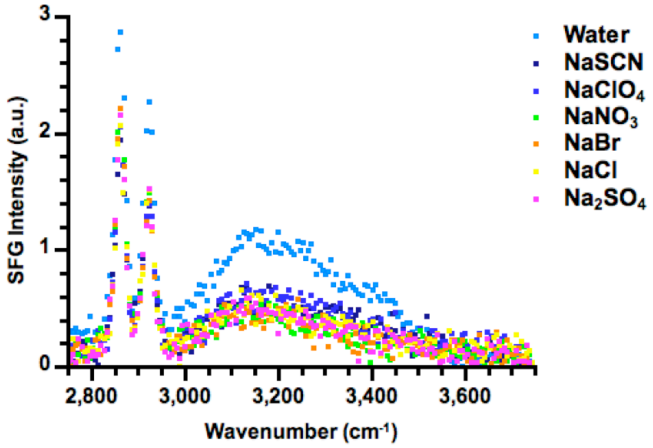

Figure 4.9 OTS-covered quartz surfaces at pH 10.0 in contact with 100 mM sodium salt solutions. There are virtually no effects as the salt concentration is increased.

Interactions of Hofmeister Anions with Positively Charged Surfaces

At pH value below 5.5, the TiO_2 surface charge is positive due to protonation of the OH surface groups. At pH 2.3, the VSFS water spectra originate from water molecules oriented with their oxygen atoms towards the positively charged surface. The pure water spectrum is shown at the topmost of Figure 4.10 spectra, for which the 3200

cm^{-1} OH stretch dominates the graph. Addition of less chaotropic anions does not alter the intensity of the water peaks, indicating the limited interaction of these ions with the surface. As more chaotropic ones make contact with the surface, the VSFS water signal becomes less prominent as a result of the more effective surface charge screening by these ions.

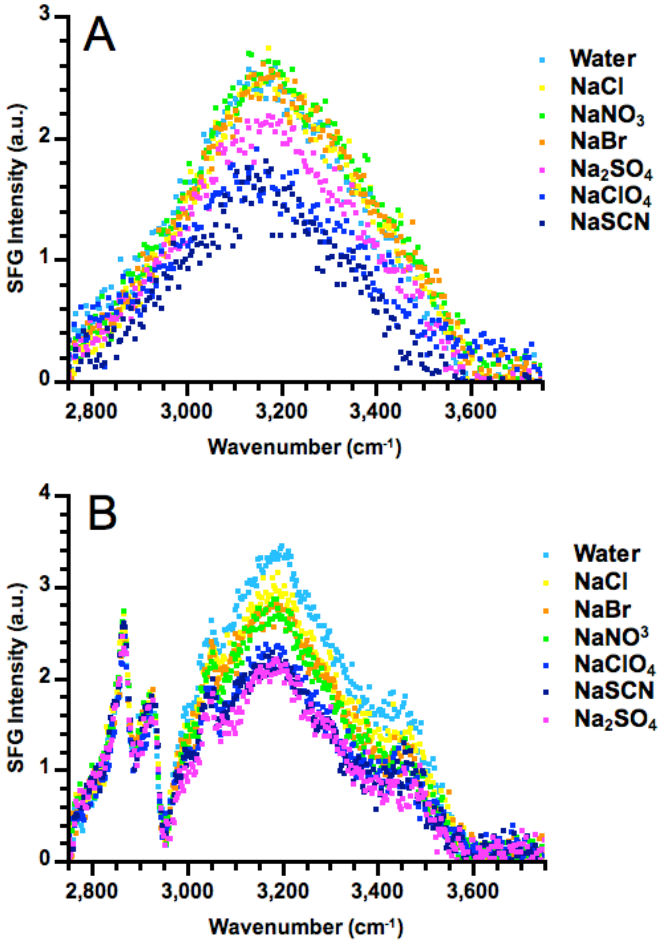

Figure 4.10 Positively charged surfaces in contact with sodium salt solutions. A) Titania surface at pH 2.3 in contact with 0.10 mM sodium salts displays a direct Hofmeister effect. B) Lysozyme Gibbs monolayers at the air/water interface with 10.0 mM sodium salt solutions as subphases, display a direct Hofmeister effect.

At pH 2.3, there is already a significant amount of chloride ions from the HCl used to adjust the pH, which are competing for adsorption with the ions under study. However, the spectra demonstrate a preferred interaction of SCN^- and ClO_4^- despite the presence of additional chloride ions. The order of interaction of anions with purely hydrophilic and positively charged surfaces follows a direct Hofmeister series, where SCN^- and ClO_4^- interact stronger to quench the VSFS water signal more effectively, followed by SO_4^{2-}, Br^-, NO_3^- and Cl^-.

Figure 4.10B shows the data for lysozyme solutions at the air/water interface. The spectra feature the CH stretch region with two peaks at 2870 cm^{-1} and 2920 cm^{-1}, which correspond to CH_3 symmetric and CH_2 asymmetric modes from the hydrophobic residues at the interface. An additional feature at 3050 cm^{-1} corresponds to the vibrational stretch from phenylalanine groups in the protein. The OH region presents the 3200 cm^{-1} and 3450 cm^{-1} water peaks that originate from water molecules that are oriented by the positive charge of the protein, similarly to the positively charged TiO_2 surface. The water spectrum in the absence of salt gives rise to the most intense VSFS signal. Upon addition of anions, the overall intensity is reduced similarly to the effects of anions on TiO_2 at low pH. The interaction of anions follows a direct Hofmeister series in which SO_4^{2-}, SCN^- and ClO_4^- quench the signal more effectively, followed by NO_3^-, Br^-, and Cl^-. Similarly to the OTS covered surfaces, SO_4^{2-} ion demonstrates the most chaotropic behavior as it interacts with lysozyme, comparable to SCN^- and ClO_4^-. The results agree with previous observations of SO_4^{2-} behaving as chaotrope in polar systems. Overall, these observations are in agreement with previous model of anion

interaction with lysozyme at low salt concentrations, in which charge screening by chaotropes is the main factor contributing to the overall inverse effect on the cloud point temperature of for the liquid-liquid phase transition of the protein.[29] The results with positively charged surfaces, further demonstrate that the interaction of anions still follows a direct Hofmeister order, with chaotropes interacting preferentially. Therefore changing the sign of the surface charge from negative to positive does not invert the preferred order of interaction with the surfaces. The apparent effect on water structure is inverted, but the anion interaction is still direct.

Conclusion

Results demonstrate that interaction of anions follows a direct Hofmeister series for both negative and positively charged surfaces regardless of degree of hydrophilicity. Although the effects on the VSFS water spectra appear to be inversed at positively charged surfaces, the anion interaction is still direct and favored for more chaotropic anions. Similarly, going from a purely hydrophilic surface to a more hydrophobic one does not alter the direct order of interaction of anions with surfaces.

CHAPTER V

CATIONIC HOFMEISTER EFFECTS ON NEGATIVELY CHARGED HYDROPHILIC SOLID SURFACES

Cations and Inorganic Surfaces

Inorganic cations and hydrophilic surfaces like quartz and TiO_2 are not only good model systems for studying the Hofmeister series,[84-86] but are also of practical importance due to their relevance in processes like quartz dissolution, chemical polishing for the manufacturing of piezoelectric devices, sensor design, separations, and tribology.[87-93] For example, it has been commonly observed that smaller monovalent cations such as Li^+ and Na^+ lead to higher dissolution rates of the substrate.[88,89] Studies performed to model hydrothermal environments for geological and environmental applications, have attempted to correlate the cations' ability to increase the quartz dissolution rate with an ion's adsorption strength on the silica surface.[94] Such studies may also be relevant for the mining, metallurgic and petroleum industries, as well as for geosciences. In particular, better understanding of cation-oxide interactions may help provide a molecular level understanding of the dissolution of silica and other oxides.[95-97]

Experimental Methods

Preparation of Hydrophilic Surfaces

Quartz and TiO_2 surfaces were prepared by following standard procedures,[61] which were described in Chapter IV.

Preparation of Salt Solutions

Salt solutions were prepared in deionized water obtained from a Millipore filtration system (18MΩ·cm; NANOpure Ultrapure Water System, Barnstead, Dubuque, IA) by dissolving the appropriate amount of high purity inorganic salt to form 0.10 M stock solutions of $ZnCl_2$, $MgCl_2$, $CaCl_2$, LiCl, NaCl, KCl, NH_4Cl, RbCl, and CsCl (99+% Sigma-Aldrich Co.). The lower concentration salt solutions used in the VSFS experiments were prepared by further diluting the stock solutions to 0.033 mM – 1.00 mM. It should be noted that micromolar salt concentrations are sufficient to perturb the water structure at the solid/liquid interface[80] and are essential to observe the maximum differences amongst the various cations. The concentrations of $MgCl_2$, $CaCl_2$, and $ZnCl_2$, were one third of those chosen for the monovalent cations in order to match the ionic strength between the monovalent and divalent systems.

It is important to point out that Zn^{2+} was only studied at a concentration of 0.033 mM. Under these conditions the solubility product, which involves formation of zinc hydroxide, can be neglected.[98-99] Therefore, in the present experiments, the effects of Zn^{2+} are due to cation adsorption to the surface rather than the change in the pH of the solution.

The pH was adjusted by using NaOH to pH 10.0, which corresponds to a total NaOH concentration of 0.10 mM in solution. This pH value is well above the pH values for the isoelectric points of the quartz and TiO_2 surfaces as demonstrated previously in Chapter IV. It was chosen to maximize the amount of deprotonated OH surface groups, while keeping the background salt concentration reasonably low. However, it should be noted that in the present experiments there was always a 0.10 mM background of Na^+ at pH 10.0, which also contributed to the apparent specific cation effects, in addition to the cation in interest. This concentration of Na^+ was kept constant in all cases; therefore, the differences observed in the VSFS water spectra reflect the specific cation effects for the various salts.

Finally, these studies mainly concern the effects of metal cations; however, NH_4^+ was also employed. It should be noted that at pH 10.0, there is only 15% of ammonium salt existing in the form of ammonium (NH_4^+) in solution; the rest 85% exists in the deprotonated form of ammonia (NH_3).

Results

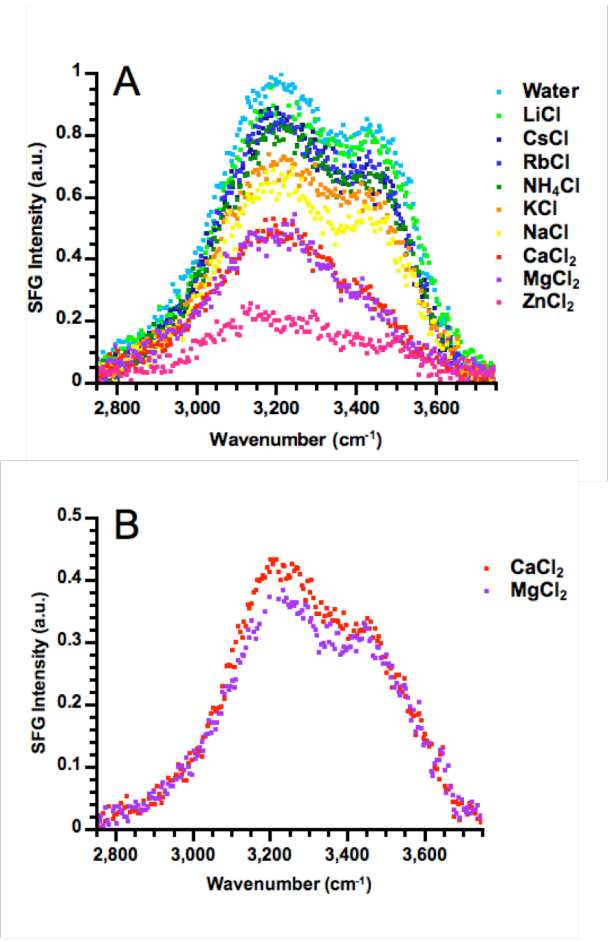

Figure 5.1. Specific cation effects on quartz surfaces at pH 10.0. (A) The VSFS spectra of the quartz surface in contact with 0.10 mM chloride solutions containing various cations. The concentration was lowered to 0.033 mM for the divalent cations. (B) VSFS spectra of quartz surfaces in contact with 1.0 mM chloride salt solutions, containing Ca^{2+} and Mg^{2+}.

Figure 5.1A shows the VSFS spectrum of water (light blue data points) in contact with amorphous quartz at pH 10.0. The OH stretch features near ~3200 cm^{-1} and ~3450 cm^{-1} reflect tetrahedral water structure and less coordinated water structure, respectively.[53] The pH 10 water spectrum in the absence of additional salt gives rise to

the highest VSFS intensity due to its lower ionic strength. As such, charge screening effects are the smallest for this system. VSFS results are also shown for the quartz surface in contact with nine chloride salt solutions at the same pH. The salt solution spectra demonstrate that the intensity for the water structure is attenuated by cations in a chemically specific fashion. The VSFS signal decrease reflects the extent of the interaction of each cation with the quartz surface, due to partial neutralization of the negative charge by the positively charged ions as well as through screening effects. The intensity of the water peaks follows a direct Hofmeister series. Specifically, divalent cations like Zn^{2+} adsorb preferentially to the solid surface, followed by Mg^{2+} and Ca^{2+}, then by the monovalent cations Na^{+}, K^{+}, NH_4^{+}, Rb^{+}, Cs^{+}, and Li^{+}. In addition, the spectra for the divalent cations were obtained at 1.0 mM salt concentration (Figure 5.1B), which was found to be the optimal concentration for observing differences between Mg^{2+} and Ca^{2+}. As can be seen in Figure 5.1B, Mg^{2+} attenuates more strongly the water signal, compared with Ca^{2+}.

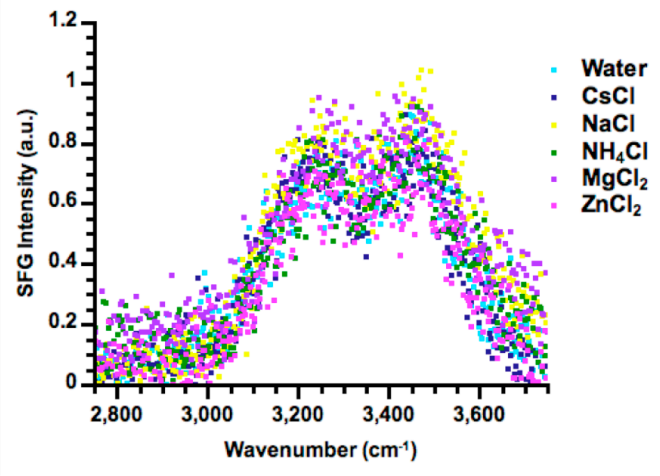

Figure 5.2. Specific cation effects on quartz surfaces at pH 6.5. The VSFS spectra of the quartz/water interface with 0.10 mM monovalent chloride salts and 0.033 mM divalent chloride salts.

Next, control experiments were performed in the absence of 0.1 mM NaOH. Under these conditions, the aqueous solution is near neutral pH and the quartz/water interface is significantly less deprotonated. As can be seen in Figure 5.2, the addition of 0.033 mM to 0.10 mM chloride salts to this system has a much less pronounced effect on the water structure and any ion specific differences were close to the limit of the experimental error. Such a result indicates that a negatively charged surface is critical to the differential attraction of the various Hofmeister cations.

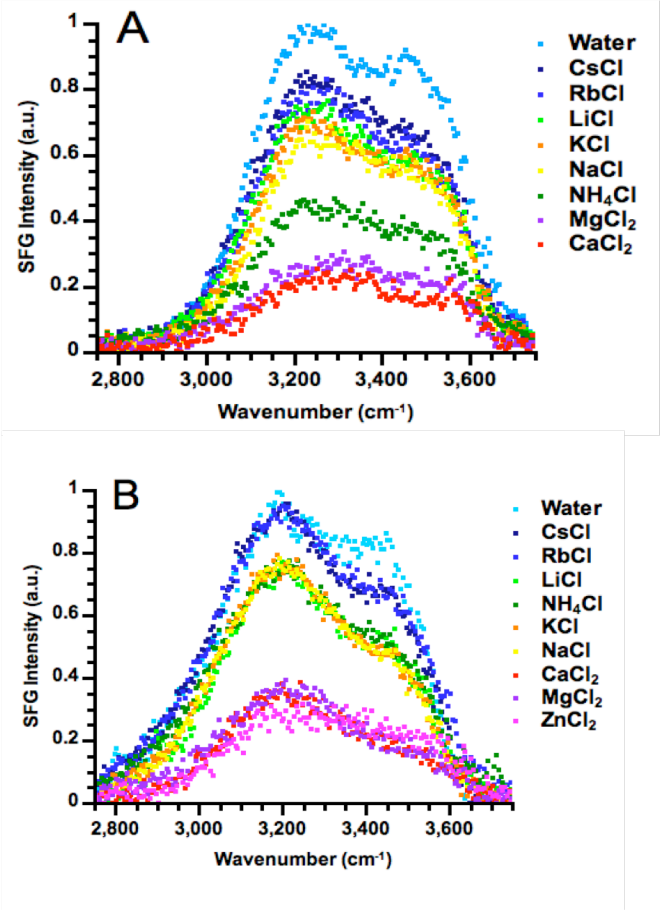

Figure 5.3. Specific cation effects on TiO_2 surfaces. (A) VSFS spectra for TiO_2 surfaces at pH 10.0 in contact with 1.0 mM chloride salt solutions containing various cations. (B) VSFS spectra for TiO_2 surfaces in contact with 0.10 mM cations.

Figure 5.3A shows VSFS data of the TiO_2/aqueous interface at pH 10.0 with 0.33 mM divalent and 1.0 mM monovalent chloride salts. The spectra clearly show the preferred interactions of divalent cations with the surface. In this case, Ca^{2+} attenuates the water signal more fully than Mg^{2+}, followed by the monovalent cations NH_4^+, Na^+,

K^+, Li^+, Rb^+ and Cs^+. Figure 5.3B shows the same systems, but with 0.1 mM chloride salts. These latter conditions match those employed at the quartz/water interface (Figure 5.1A). In this case, one observes much less pronounced differences between Ca^{2+} and Mg^{2+}; however, Zn^{2+} still appears to attenuate the water signal slightly more strongly than the other divalent cations. It also becomes more difficult to discern the differences amongst NH_4^+, K^+, Na^+, and Li^+.

Discussion

Deprotonated OH groups at oxide surfaces are a key factor in determining the extent of cation adsorption and double layer screening, since the oxygen is the putative interaction site for cationic species. Both TiO_2 and quartz become more negatively charged as the pH is raised and it has been demonstrated that adsorption of most cations is favored at high pH.[100,101] For these oxides, there are obvious differences in the trends for interfacial cation partitioning as seen in Figures 5.1 and 5.3. This may be related to the basicity and polarizability of the surface sites.

The adsorption of cations on quartz surfaces at high pH generally follows a direct Hofmeister series, dominated by trends related to ion size, net charge, and charge density (Figure 5.1). The smaller divalent and monovalent cations have a higher charge density than larger monovalent cations.[24,102] In the case of the divalent ions, Zn^{2+} and Mg^{2+} are very similar in size. Their differences in adsorption should be related to their relative affinities for hydroxides. In fact, the hydrolysis equilibrium constant value (K_1) for $Zn(OH)^+$ is larger than the one for $Mg(OH)^+$.[103] In other words, Zn^{2+} forms tighter complexes with hydroxide. The solubility products (K_{sp}) in alkaline solutions for the

three divalent cations used in this study follow the order $Zn^{2+} < Mg^{2+} < Ca^{2+}$.[36,37] Therefore, a divalent cation's propensity for surface segregation at the quartz/water interface appears to be directly correlated with its propensity for complexation with hydroxide anions. This order is also observed for divalent cations with similar hydrophilic substrates like mica.[104]

The series for monovalent cations is Na^+, K^+, NH_4^+, Rb^+, Cs^+, and Li^+ on quartz, which mostly corresponds to a decreasing charge density trend in the monovalent series. Strikingly, Li^+ is a strong exception. In fact, it behaves like an ion of even lower charge density than Cs^+ and Rb^+. Indeed, Li^+ is strongly hydrated in aqueous solutions.[105-110] As such, water molecules are tightly bound, especially within the first hydration shell. As the effective charge density for Li^+ is decreased by its hydration waters, the surrounding water molecules to become polarized.[110] Therefore, it behaves like a large, cation with low charge density. Similar anomalous behavior was predicted with potentials of mean force simulations at the air/water interface.[111]

Key differences between quartz and TiO_2 involves the dielectric constant and polarizability of the two substrates. TiO_2, which is a semiconductor, has a much larger dielectric constant and it is more polarizable than quartz.[112,113] The isoelectric points of the two surfaces in aqueous solution are also quite different, pH 5.5 and pH 2.0, for TiO_2 and quartz, respectively.[61,81] Therefore, cation adsorption on these substrates may be expected to be somehow different. Like quartz, the interactions of cations with TiO_2 still follow the same general trend based upon an ion's net charge. Indeed, divalent cations adsorb preferentially compared to monovalent cations. However, two metal cations, Li^+

and Ca^{2+}, show distinct behavior on TiO_2 compared with quartz (Figure 5.3A). On TiO_2, Li^+ behaves in a fashion, which is intermediate between Rb^+ and K^+. Similarly, Ca^{2+} and Mg^{2+} switch places in the Hofmeister series on TiO_2 as compared with quartz (Figure 5.1A). Thus, the properties of the substrate appear to be crucial factor in the Hofmeister ordering of cations. Specifically, the more polarizable, semiconductor substrate, TiO_2, shows greater deviations from a direct Hofmeister series. Such properties may be important in the field of biomaterials containing TiO_2. Indeed, the preferential interaction of this ion on this surface is believed to favor osteoblast development, bone growth, and protein adsorption on implants made of titanium, which typically has a thin TiO_2 coating *in vivo*.[114-118]

Next, it should be noted that the position of NH_4^+ in the Hofmeister series with TiO_2 is also significantly shifted compared with quartz. In fact, it adsorbs more strongly than any other monovalent cation on this substrate (Figure 5.3A). This behavior deviates from the expected Hofmeister series and should be related to the increased ability of TiO_2 to serve as a hydrogen bond acceptor. As noted above, TiO_2 is a more basic oxide than quartz. Due to the greater electropositive nature of the Ti atom compared with the Si atom, the oxygen atoms in TiO_2 are more electronegative and more likely to form hydrogen bonds with species like NH_4^+ ions.[119] Therefore, the adsorption of NH_4^+ on TiO_2 is not only dictated by its charge density, but also by its hydrogen bonding ability.[120] It should be noted that NH_3 is also present in the solutions in contact with quartz and TiO_2. However, since this molecule does not bear a positive charge, it should have far less influence on the 3200 cm^{-1} peak in the SFG spectrum, which is closely

related to the interfacial electric fields. Moreover, NH_4^+ should accumulate at the negatively charged oxide interface to a much greater extent than the neutral NH_3. This idea agrees with calculated values of the adsorption energies of these two species.[120] Also, proton donation from NH_4^+ ions is more facile than from NH_3, making such adsorption even more favorable to the TiO_2 surface.[120]

In summary, the effects of Zn^{2+}, Mg^{2+}, Ca^{2+}, NH_4^+, Li^+, Na^+, K^+, Rb^+, and Cs^+ ions on the water structure adjacent to negatively charged solid surfaces have been explored using VSFS at the oxide/aqueous interface. It was observed that at pH 10.0, and 0.033 mM to 1.0 mM salt concentrations, the effects of the cations on the interfacial water structure were ion specific and mostly followed a rank ordering in line with their charge density. Specific ion effects were less pronounced on less negatively charged surfaces. For both quartz and TiO_2, the results demonstrated that the interactions of cations followed a direct Hofmeister series with a greater number of exceptions on TiO_2 than on quartz. The divergence in the ordering of the cations on TiO_2 may be explained by the substrates electronic properties, charge density, and hydrogen bonding ability. Such insights may help provide information about how cations interact with more complex biological systems.

CHAPTER VI

CONCLUSIONS

The understanding of complex interfacial phenomena has been facilitated as science grows in sophistication, and new analytical tools are available and applied to study interfaces. However, due to the complexity of interfacial systems, especially those involving macromolecules like polymers, peptides, and proteins, it is necessary to emphasize the importance of simpler systems as starting points in research in order to be able to elucidate more intricate processes.

It is now clear that accumulation of ions is favored at interfaces, in which they play crucial roles by influencing all types of physical phenomena. A full understanding of the mechanisms by which ions affect water at surfaces, and interact with the molecules dissolved in it is still under development, but it is now obvious that generally those mechanisms are similar for both biological and inorganic systems.

The observation of specific ion effects presented in this thesis was greatly facilitated by the use of vibrational sum frequency spectroscopy. At the air/water interface, it is quite challenging to interpret results, particularly when biomolecules are present in solution due to the complexity of the resulting vibrational spectra. However, we have been able to effectively use vibrational sum frequency spectroscopy in presence of monolayers of model protein bovine serum albumin, elastin-like peptides and surfactants, and by analyzing the intensity of water structure, we have been able to learn about the extent of the interaction of anions with these macromolecules, and elucidate

the electrostatic nature of the interaction. We were able to prove that specific anion effects on water structure are dominated by the charge state of the interfacial layer, rather than the detailed chemical structure of the macromolecules. The results pose clear evidence for the direct interaction of anions with the macromolecule's surface, and represent additional proof to completely rule out the originally proposed water mediated mechanism. At the solid/liquid interface, we were able to confirm that the propensities of anions to adsorb at interfaces of varying charge sign are favored for more polarizable anions, following the direct Hofmeister order. These results are relevant to disprove the notion that the order of the interaction can be inverted with changes in charge sign or degree of hydrophobicity of the surface, which has been a common idea in recent theoretical studies that attempt to explain the molecular level details in observed inverse effects, like that of lysozyme.

Similarly, our study on cation interactions with metal oxide surfaces is one of the very first systematic studies that provides with direct molecular level information, despite the known challenge of cations displaying weak effects, which generally have made studies difficult to execute. The specific cation effects are quite prominent at the charged oxide surfaces, and the data presents a unique starting point for understanding the interaction of cations with more complex systems like peptides and proteins, in which experiments will need careful design and data analysis in order to be able to obtain reliable information on the interactions and their influence in more complex phenomena. For example, our observations on the effects of polarizability of putative binding groups for cations can be further examined and compared by using negatively

charged elastin-like peptides. In these peptides, carboxylate moieties from amino acids are the sites responsible for cation adsorption. Additionally, these carboxylate groups are much more polarizable than the hydroxyl groups in titanium oxide, and even more than those in silicon oxide surfaces. Interestingly, recent results[121] in our laboratory are demonstrating that the carboxylate moieties are even more effective in interacting with ions like lithium. There is an overall common trend in which as the polarizability of the binding sites increases, the adsorption of lithium, ammonium and calcium is even more favored.

By proving the generality of ion interactions beyond biological, we can help facilitate the understanding of the myriad of systems where ions play important roles, and we can provide future scientists with basic information to aid the development of solutions to current and future technological challenges.

REFERENCES

(1) Kunz, W. *Curr. Opin. Coll. Interf. Sci.* **2010**, *15*, 34-39.

(2) Zhang, Y.; Cremer, P. S. *Curr. Opin. Chem. Biol.* **2006**, *10*, 658-66.

(3) Broering, J. M.; Bommarius, A. S. *J. Phys. Chem. B* **2005**, *109*, 20612-20619.

(4) Xiong, K., Asciutto, E. K., Madura, J. D.; Asher, S. A. *Biochemistry* **2009**, *48*, 10818-10826.

(5) Pinna, M. C., Bauduin, P., Touraud, D., Monduzzi, M., Ninham, B. W.; Kunz, W. *J. Phys. Chem. B* **2005**, *109*, 16511-16514.

(6) Pinna, M. C., Salis, A., Monduzzi, M.; Ninham, B. W. *J. Phys. Chem. B* **2005**, *109*, 5406-5408.

(7) Bauduin, P., Nohmie, F., Touraud, D., Neueder, R., Kunz, W.; Ninham, B. W. *J. Mol. Liq.* **2006**, *123*, 14-19.

(8) Vrbka, L., Jungwirth, P., Bauduin, P., Touraud, D.; Kunz, W. *J. Phys. Chem. B* **2006**, *110*, 7036-7043.

(9) Perez-Jimenez, R., Godoy-Ruiz, R., Ibarra-Molero, B.; Sanchez-Ruiz, J. M. *Biophys. J.* **2004**, *86*, 2414-2429.

(10) Curtis, R. A.; Lue, L. *Chem. Eng. Sci.* **2006**, *61*, 907-923.

(11) Collins, K. D. *Methods* **2004**, *34*, 300-311.

(12) Lo Nostro, P., Ninham, B. W., Milani, S., Fratoni, L.; Baglioni, P. *Biopolymers* **2006**, *81*, 136-148.

(13) Lo Nostro, P., Ninham, B. W., Lo Nostro, A., Pesavento, G., Fratoni, L.; Baglioni, P. *Phys. Biol.* **2005**, *2*, 1-7.

(14) Ninham, B. W.; Yaminsky, V. *Langmuir* **1997**, *13*, 2097-2108.

(15) Bostrom, M., Kunz, W.; Ninham, B. W. *Langmuir* **2005**, *21*, 2619-2623.

(16) Srinivasan, V.; Blankschtein, D. *Langmuir* **2003**, *19*, 9932-9945.

(17) Srinivasan, V.; Blankschtein, D. *Langmuir* **2003**, *19*, 9946-9961.

(18) Bostrom, M., Williams, D. R. M.; Ninham, B. W. *Langmuir* **2002**, *18*, 6010-6014.

(19) Hennig, A., Fischer, L., Guichard, G.; Matile, S. *J. Am. Chem. Soc.* **2009**, *131*, 16889-16895.

(20) Sovago, M., Wurpel, G. W. H., Smits, M., Muller, M.; Bonn, M. *J. Am. Chem. Soc.* **2007**, *129*, 11079-11084.

(21) Aroti, A., Leontidis, E., Maltseva, E.; Brezesinski, G. *J. Phys. Chem. B* **2004**, *108*, 15238-15245.

(22) Zhang, Y. J., Furyk, S., Bergbreiter, D. E.; Cremer, P. S. *J. Am. Chem. Soc.* **2005**, *127*, 14505-14510.

(23) Zhang, Y. J., Furyk, S., Sagle, L. B., Cho, Y., Bergbreiter, D. E.; Cremer, P. S. *J. Phys. Chem. C* **2007**, *111*, 8916-8924.

(24) Lo Nostro, P.; Fratoni, L.; Ninham, B. W.; Baglioni, P. *Biomacromolecules* **2002**, *3*, 1217-1224.

(25) Bostrom, M.; Tavarez, F. W.; Bratko, D.; Ninham, B. W. *Prog. Colloid Polym. Sci.* **2006**, *133*, 74-77.

(26) Hofmeister, F. *Arch. Exp. Pathol. Pharmakol.* **1888**, *24*, 247-260.

(27) Chen, X.; Yang, T.; Kataoka, S.; Cremer, P. S. *J. Am. Chem. Soc.* **2007**, *129*, 12272-12279.

(28) Kunz, W.; Henle, J.; Ninham, B. W. *Curr. Opin. Colloid Interface Sci.* **2004**, *9*, 19-37.

(29) Zhang, Y; Cremer, P. S. *Proc. Natl. Acad. Sci.* **2009**, *106*, 15249-15253.

(30) Chen, X.; Flores, S. C.; Lim, S. - M .; Zhang, Y.; Yang, T.; Kherb, J.; Cremer. P. S. *Langmuir* **2010**, *26*, 16447-16454.

(31) Tobias, D. J.; Hemminger, J. C. *Science* **2008**, *319*, 1197-1198.

(32) Pegram, L. M.; Wendorff, T.; Erdmann, R.; Shkel, I.; Bellissimo, D.; Felitsky, D. J.; Record Jr. M. T. *Proc. Natl. Acad. Sci.* **2010**, *107(17)*, 7716-7721.

(33) Klasczyk, B.; Knecht, V.; Lipowsky, R.; Dimova, R. *Langmuir* **2010**, *26*(24), 18951-18958.

(34) Kunz, W.; Lo Nostro, P.; Ninham, B. W. *Curr. Op. Colloid and Interface Sci.* **2004**, *9*, 1-18.

(35) Zhang, Y.; Cremer, P. S. *Curr. Opin. Chem. Biol.* **2006**, *10*, 658-663.

(36) Jungwirth, P.; Tobias, D. J. *J. Phys. Chem. B*, **2002,** *106*, 6361-6373.

(37) Smith, J. D., Saykally, R. J.; Geissler, P. L. *J. Am. Chem. Soc.* **2007**, *129*, 13847-13856.

(38) Cho, Y.; Zhang, Y.; Christensen, T.; Sagle, L. B.; Chilkoti, A.; Cremer, P. S. *J. Phys. Chem. B* **2008**, *112*, 13765-13771.

(39) Jungwirth, P. *Faraday Discuss.* **2009**, *141*, 9-30.

(40) Schwierz, N.; Horinek, D.; Netz, R. R. *Langmuir* **2010**, *26(10)*, 7370-7379.

(41) Zhang, Y.; Cremer, P. S. *Ann. Rev. Phys. Chem.* **2010**, *61*, 63-83.

(42) Jungwirth, P; Tobias, D. J. *J. Phys. Chem. B* **2001**, *105*, 10468-10472.

(43) Jungwirth, P.; Tobias, D. J. *J. Phys. Chem. B* **2002**, *106*, 6361-6373.

(44) Jungwirth, P.; Winter, B. *Annu. Rev. Phys. Chem.* **2008**, *59*, 343-366.

(45) Pegram, L. M.; Record, M. T. *Proc. Natl. Acad. Sci. U.S.A.* **2006**, *103*, 14278-14281.

(46) Pegram, L. M.; Record, M. T. *J. Phys. Chem. B* **2007**, *111*, 5411-5417.

(47) Pegram, L. M.; Record, M. T. *J. Phys. Chem. B* **2008**, *112*, 9428-9436.

(48) Gurau, M. C., Lim, S. M., Castellana, E. T., Albertorio, F., Kataoka, S.; Cremer, P. S. *J. Am. Chem. Soc.* **2004**, *126*, 10522-10523.

(49) Ries-Kautt, M. M.; Ducruix, A. F. *J. Biol. Chem.* **1989**, *264*, 745-748.

(50) Bostrom, M.; Tavares, F.W.; Finet, S.; Skouri-Panet, F.; Tardieu, A.; Ninham, B.W. *Biphys. Chem.* **2005**, *117*, 217-224.

(51) Shen, Y. R. *The Principles of Nonlinear Optics*; John Wiley & Sons: New York, 1984.

(52) Shen, Y. R. *Nature* **1989**, *337*, 519-525.

(53) Du, Q.; Freysz, E.; Shen, Y. R. *Phys. Rev. Lett.* **1994**, *72*, 238-241.

(54) Kim, J.; Kim, G.; Cremer, P.S. *Langmuir* **2001**, *17*, 7255-7260.

(55) Gopalakrishnan, S.; Liu, D. F.; Allen, H. C.; Kuo, M.; Shultz, M. J. *Chem. Rev.* **2006**, *106*, 1155-1175.

(56) Shen, Y. R.; Ostroverkhov, V. *Chem. Rev.* **2006**, *106*, 1140-1154.

(57) Richmond, G. L. *Chem. Rev.* **2002**, *102*, 2693-2724.

(58) Du, Q.; Freysz, E.; Shen, Y. R. *Science,* **1994**, *264*, 826-828.

(59) Du, Q.; Superfine, R.; Freysz, E.; Shen, Y. R. *Phys. Rev. Lett.* **1993**, *70*, 2313-2316.

(60) Fan, Y.; Chen, X.; Yang, L.; Cremer, P. S.; Gao, Y. Q. *J. Phys. Chem. B* **2009,** *113,* 11672-11679.

(61) Kataoka, S.; Gurau, M. C.; Albertorio, F.; Holden, M. A.; Lim, S.-M.; Yang, R. D.; Cremer, P. S. *Langmuir* **2004**, *20*, 1662-1666.

(62) Shen, Y. R. *Solid State Comm.* **1998**, *108*, 399-406.

(63) Lu, J. R.; Su, T. J.; Thomas, R. K. *J. Colloid. Inter. Sci.* **1999**, *213(2)*, 426-437.

(64) Lu, J. R., Su, T. J.; Penfold, J. *Langmuir* **1999**, 15, 6975-6983.

(65) Tanford, C., Swanson, S. A.; Shore, W. S. *J. Am. Chem. Soc.* **1955**, *77*, 6414-6421.

(66) Chen, X.; Sagle, L. B.; Cremer, P. S. *J. Am. Chem. Soc.* **2007**, *129*, 15104-15105.

(67) Adamson, A. W.; Gast, A. P. *Physical Chemistry of Surfaces*; Wiley: New York, 1997.

(68) Meyer, D. E.; Chilkoti, A. *Biomacromolecules* **2004**, *5*, 846-851.

(69) Meyer, D. E.; Chilkoti, A. *Biomacromolecules* **2002**, *3*, 357-367.

(70) Wang, J., Buck, S. M.; Chen, Z. *J. Phys. Chem. B* **2002**, *106*, 11666-11672.

(71) Kim, G., Gurau, M., Kim, J.; Cremer, P. S. *Langmuir* **2002**, *18*, 2807-2811.

(72) Marcus, Y. *Ion Properties*; Marcel Dekker, Inc.: New York, 1997.

(73) Flores, S. C.; Kherb, J.; Cremer, P. S. *In preparation.*

(74) Tadeo, X., Pons, M.; Millet, O. *Biochemistry* **2007**, *46*, 917-923.

(75) Gopalakrishnan, S., Liu, D. F., Allen, H. C., Kuo, M.; Shultz, M. J. *Chem. Rev.* **2006**, *106*, 1155-1179.

(76) Richmond, G. L. *Chem. Rev.* **2002**, *102*, 2693-2724.

(77) Romero, C.; Moore, H. J.; Lee, T. R.; Baldelli, S. *J. Phys. Chem. C* **2007**, *111*, 240-247.

(78) Ong, J. L. Appl. Surf. Sci. **1993**, *72*, 7-13.

(79) Quinn, R. K.; Armstrong, N. R. *J. Electrochem. Soc.* **1978**, *125*, 1790-1796.

(80) Yang, Z.; Li, Q.; Chou, K. C. *J. Phys. Chem. C* **2009**, *113*, 8201-8205.

(81) Iller, R. K. *The Surface Chemistry of Silica*, 30th ed.; John Wiley & Sons: New York, 1979; pp 622 -656.

(82) Ye, S.; Nihonyanagi, S.; Uosaki, K. *Phys. Chem. Chem. Phys.* **2001**, *3*, 3463-3469.

(83) Pegram, L. M.; Record Jr., M. T. *Chem. Phys. Lett.* **2008**, *467*, 1-8.

(84) Salis, A.; Boström, M.; Medda, L.; Parsons, D. F.; Barse, B.; Monduzzi, M.; Ninham, B. W. *Langmuir* **2010**, *26*, 2484-2490.

(85) Dove, P. M.; Craven, C. M. *Geochim. Cosmochim. Acta* **2005**, *69*, 4963-4970.

(86) Malati, M. A. *Surf. Coat. Tech.* **1987**, *30*, 317-325.

(87) Deleuze, M.; Goiffon, A.; Ibañez, A.; Philippot, E. *J. Solid State Chem.* **1995**, *118*, 254-260.

(88) Deleuze, M.; Goiffon, A.; Ibañez, A.; Philippot, E. *J. Mater. Sci.* **1996**, *31*, 2123-2130.

(89) Moldovan, C.; Iosub, R.; Modreanu, M. *Int. J. Inorg. Mater.* **2001**, *3*, 1173-1176.

(90) Stux, A. M.; Meyer, G. J. *J. Fluoresc.* **2002**, *12*, 419-423.

(91) Tani, K.; Kubojima, H. *Chromatographia* **1998**, *47*, 655-658.

(92) Donose, B. B.; Vakarelski, I. U.; Higashitani, K. *Langmuir* **2005**, *21*, 1834-1839.

(93) Pashley, R. M. *J. Colloid Interface Sci.* **1981**, *83*, 531-546.

(94) Dove, P. M.; Crerar, D. A. *Geochim. Cosmochim. Acta* **1990**, *54*, 955-969.

(95) Ishikawa, K.; Yoshioka, T.; Sato, T.; Okuwaki, A. *Hydrometallurgy* **1997**, *45*, 129-135.

(96) Paige, C. R.; Kornicker, W. A.; Hileman, O. E. Jr. *J. Radioanal. Nucl. Chem.* **1992**, *159*, 37-46.

(97) Farrow, J. B.; Horsley, R. R.; Meagher, L.; Warren, L. J. *J. Rheol.* **1989**, *33*, 1213-1230.

(98) Shkol'nikov, E. V. *Russ. J. Appl. Chem.* **2004**, *77*, 1255-1258.

(99) Packter, A. *Cryst. Res. Technol*. **1981**, *16*, 1273-1281.

(100) Loewenstein, L. M.; Mertens, P. W. *J. Electrochem. Soc.* **1998**, *145*, 2841-2847.

(101) Dugger, D. L.; Stanton, J. H.; Irby, B. N.; McConnell, B. L.; Cummings, W. W.; Maatman, R. W. *J. Phys. Chem.* **1964**, *68*, 757-760.

(102) Collins. K. D. *Biophys. J.* **1997**, *72*, 65-76.

(103) Burgess, J. *Ions in Solution: Basic Principles of Chemical Interactions*; Horwood Publishing Limited: Chichester, 1999.

(104) Parsons, D. F.; Ninham, B. W. *Langmuir* **2010**, *26*, 6430-6436.

(105) Varma, S.; Rempe, S. B. *Biophys. Chem.* **2006**, *124*, 192-199.

(106) Rudolph, W.; Brooker, M. H.; Pye, C. C. *J. Phys. Chem.* **1995**, *99*, 3793-3797.

(107) Wachter, W.; Fernández, S.; Buchner, R.; Hefter, G. *J. Phys. Chem. B* **2007**, *111*, 9010-9017.

(108) Ansell, S.; Barnes, A. C.; Mason, P. E.; Neilson, G. W.; Ramos, S. *Biophys. Chem.* **2006**, *124*, 171-179.

(109) Lyubartsev, A. P.; Laasonen, K.; Laaksonen, A. *J. Chem. Phys.* **2001**, *114*, 3120-3126.

(110) Loeffler, H. H.; Rode, B. M. *J. Chem. Phys.* **2002**, *117*, 110-117.

(111) Horinek, D.; Herz, A.; Vrbka, L.; Sedlmeier, F.; Mamatkulov, S. I.; Netz, R. R. *Chem. Phys. Lett.* **2009**, *479*, 173-183.

(112) Goniakowski, J.; Bouette-Russo, S.; Noguera, C. *Surf. Sci.* **1993**, *284*, 315-327.

(113) Noguera, C.; Goniakowski, J.; Bouette-Russo, S. *Surf. Sci.* **1993**, *287/288*, 188-191.

(114) Kasemo, B. *J. Prosthet. Dent.* **1983**, *49*, 832-837.

(115) Diebold, U. *Surf. Sci. Reports* **2003**, *48*, 53-229.

(116) Nayab, S. N.; Jones, F. H.; Olsen, I. *Biomaterials* **2007**, *28*, 38-44.

(117) Ellingsen, J. E. *Biomaterials* **1991**, *12*, 593-596.

(118) Klinger, A.; Steinberg, D.; Kohavi, D.; Sela, M. N. *J. Biomed. Mater. Res.* **1997**, *36*, 387-392.

(119) Fu, Q.; Wagner, T. *Surf. Sci. Reports* **2007**, *62*, 431-498.

(120) Markovits, A.; Ahdjoudj, J.; Minot, C. *Surf. Sci.* **1996**, *365*, 649-661.

(121) Kherb, J.; Flores, S. C.; Cremer, P. S. *In preparation*.

VITA

Name: Sarah Cecilia Flores Araujo

Address: Department of Chemistry
Texas A&M University, Interdisciplinary and Life Sciences Building
301 Old Main Dr. ILSB Room 1211
College Station, TX 77843-3474

Email Address: sflores@mail.chem.tamu.edu

Education: B.S., Chemistry, University of North Texas, 2004
M.S., Chemistry, University of North Texas, 2006
Ph.D., Chemistry, Texas A&M University, 2011